PHYSICAL REVIEW D **104,** 024014 (2021)

Time-domain metric reconstruction for hyperbolic scattering

Oliver Long and Leor Barack
Mathematical Sciences, University of Southampton, Southampton SO17 1BJ, United Kingdom

(Received 12 May 2021; accepted 25 May 2021; published 7 July 2021)

Self-force methods can be applied in calculations of the scatter angle in two-body hyperbolic encounters, working order by order in the mass ratio (assumed small) but with no recourse to a weak-field approximation. This, in turn, can inform ongoing efforts to construct an accurate model of the general-relativistic binary dynamics via an effective-one-body description and other semianalytical approaches. Existing self-force methods are to a large extent specialized to bound, inspiral orbits. Here, we develop a technique for (numerical) self-force calculations that can efficiently tackle scatter orbits. The method is based on a time-domain reconstruction of the metric perturbation from a scalarlike Hertz potential that satisfies the Teukolsky equation, an idea pursued so far only for bound orbits. The crucial ingredient in this formulation is certain jump conditions that (each multipole mode of) the Hertz potential must satisfy along the orbit, in a $1+1$-dimensional multipole reduction of the problem. We obtain a closed-form expression for these jumps, for an arbitrary geodesic orbit in Schwarzschild spacetime, and present a full numerical implementation for a scatter orbit. In this paper, we focus on method development and go only as far as calculating the Hertz potential; a calculation of the self-force and its physical effects on the scatter orbit will be the subject of forthcoming work.

DOI: 10.1103/PhysRevD.104.024014

I. INTRODUCTION

The post-Minkowskian (PM) theory of two-body dynamics in General Relativity has seen a rapid progress in recent years, thanks in part to the introduction of radically new approaches to the problem. These include the effective-one-body method [1–4], effective-field-theory treatments [5–8], and the use of dictionaries that translate between quantum scattering amplitudes and classical gravitational dynamics ("double copy") [9–12]. A recent milestone is the derivation of the conservative two-body dynamics through 4PM order [$O(G^4)$] using scattering-amplitude methods [13], and there is also progress on the description of radiative effects [13–15].

An alternative route to high-order PM calculations is provided by black-hole perturbation theory, i.e., methods that rely on an expansion in the mass ratio η of the binary, without a weak-field approximation. The remarkable effectiveness of such an avenue of approach was first noted by Damour in Ref. [3]. At least for structureless point particles, the 2PM conservative two-body dynamics can be inferred in full simply from the scatter angle of *geodesic* orbits on a Schwarzschild background (as a function of, say, the orbit's energy and impact parameter). Knowledge of the $O(\eta)$ backreaction correction to the scatter angle—the so-called first-order self-force correction—determines the full conservative dynamics through 4PM order (at any mass ratio). A second-order self-force calculation would achieve the same, to as high an order as 6PM. Furthermore, since at each order in η the self-force results are "exact" (they "contain all PM terms"), such results can provide a useful benchmark against which to assess the performance of the PM series in the strong-field regime.

Thus, there is a motivation for self-force calculations in scatter-orbit scenarios. Unfortunately, existing calculation methods and codes are to a large extent tailored to tackle bound-orbit or inspiral systems, which are relevant to astrophysical extreme mass-ratio setups and whose study remains the main driver of such calculations. These codes cannot be immediately applied to scatter-type orbits. For example, the most advanced self-force code [16] is based on a procedure of metric reconstruction from discrete frequency-mode solutions of the perturbation equations, which crucially relies on the assumption that the orbit is quasiperiodic. (Part of the issue is that the so-called "method of extended homogeneous solutions" [17], which enables the time-domain reconstruction of the metric perturbation near the particle, works *a priori* only for bounded orbits.) While these difficulties are unlikely insurmountable, existing frequency-domain methods would require much further development before they can be applied to scatter-type orbits; see Refs. [18,19] for initial work.

Time-domain treatments offer an alternative route to unbound-orbit calculations, bypassing some of the difficulties. Reference [20] recently presented a first such calculation, based on a numerical integration of the Lorenz-gauge metric perturbation equations on a Schwarzschild background, formulated as an initial-value problem in

$1+1$ dimensions. This work did not consider scatter-type orbits but considered the special case of a particle falling from rest at infinity, eventually (radiation ignored) getting trapped on an unstable circular orbit around the Schwarzschild black hole. The method could be further developed to tackle scatter orbits, but significant hurdles remain. In particular, the Lorenz-gauge formulation admits certain nonphysical, linearly growing gauge modes that develop generically in numerical evolutions and are hard to control [21]. These were tamed in Ref. [20] by exploiting the asymptotic periodicity of the special "zoom-whirl" setup, but it remains unclear how to handle the problem in the case of hyperboliclike scattering, where similar tricks cannot be used. Furthermore, the Lorenz-gauge formulation involves a rather unwieldy coupled set of partial differential equations, which impacts on computational precision and cost.

In this paper, we develop an alternative time-domain method and illustrate its implementation for scatter orbits. The method is based on metric reconstruction from a scalarlike Hertz potential, which satisfies the Teukolsky equation. The equation is solved as an evolution problem in the time domain, and the metric perturbation is then reconstructed from the solution (and additional, trivial perturbation pieces) in a gauge suitable for self-force calculations [22] (the "no-string" radiation gauge, to be reviewed in Sec. II). This procedure circumvents the main pitfalls of the Lorenz-gauge method: one has to solve a single, simple hyperbolic equation, and one encounters no problematic gauge modes.

The central idea behind our method is not new: it was introduced by one of us with Giudice in Ref. [23], where, however, it was fully developed and implemented only for circular (geodesic) orbits. Here, we formulate the method for arbitrary (geodesic) orbits and implement it numerically for scatter orbits. We go as far as computing the Hertz potential along the scatter orbit, in order to demonstrate the applicability of our method and explore its performance. We do not proceed here to calculate the self-force and its effects on the scatter angle; this we hope to accomplish soon in subsequent work.

We begin in Sec. II with a review of metric reconstruction for a point-particle source in a no-string gauge, specializing to a Schwarzschild background and casting the procedure in a form suitable for a time-domain implementation. In Sec. III, we then formulate an initial-value problem for the (no-string) Hertz potential. In the no-string construction, the spacetime outside the central black hole is split into two vacuum domains, $r > R(t)$ and $r < R(t)$, where r and t are Schwarzschild coordinates and $r = R(t)$ along the particle's trajectory. The crucial ingredient in our formulation are jump conditions that the Hertz potential and its derivatives must satisfy on the (time-dependent) 2-sphere $r = R(t)$. These conditions are derived in Sec. IV for an arbitrary timelike geodesic trajectory. This is the main new result of the formulation part of this work.

In Sec. V, we present a new code for numerical integration of the Bardeen-Press-Teukolsky (BPT) equation in $1+1$ dimensions on a Schwarzschild background. The code employs a finite-difference scheme on a characteristic grid based on Eddington-Finkelstein coordinates—a simple tried-and-tested architecture that has worked reliably in many past calculations of the Lorenz-gauge and scalar-field self-forces. We demonstrate, however, how a naive implementation of this standard scheme fails when applied to the Teukolsky equation with spin parameter $s = \pm 2$, due to divergences that develop at late time (an exponential divergence for $s = +2$ and a $\sim t^4$ divergence for $s = -2$). We attribute these divergences to certain growing modes of the Teukolsky equation. These modes violate the physical boundary conditions, but since boundary conditions are not actively imposed in our characteristic scheme, they are allowed to grow. The problem persists even in vacuum evolutions. We explain why the issue is not encountered in existing time-domain Teukolsky codes based on hyperboloidal slicing with compactification [24–26].

Here, restricting to the Schwarzschild case, we opt for a simpler solution. We circumvent the problem of growing modes by transforming to a new field variable (using a time-domain version of the Chandrasekhar transformation), which, in the vacuum case, satisfies the Regge-Wheeler (RW) equation, for which the problem does not occur. In Sec. VI, we reformulate our initial-value problem in terms of the new variable and, in particular, derive the necessary jump conditions for it on $r = R(t)$.

In Sec. VII, we finally present a full numerical implementation of our method, for a scatter orbit. We evolve the field equation for the RW-like variable and from it compute (multipole mode by multipole mode) the no-string Hertz potential along the scatter trajectory. We thus numerically construct the necessary input for a calculation of the self-force along the orbit.

We conclude in Sec. VIII by reviewing the extra steps needed to carry our the calculation of the self-force from the Hertz potential. We also discuss the prospects of extending our method to the case of a Kerr background.

Throughout this work, we use units in which $G = 1 = c$ and adopt the metric signature $(-+++)$. For quantities that arise in the Newman-Penrose formalism, we follow the sign conventions of Ref. [27], as summarized in Appendix A therein; for ease of reference, we review the relevant details here, in Appendix A, specialized to the Schwarzschild case.

II. REVIEW OF METRIC RECONSTRUCTION IN A NO-STRING RADIATION GAUGE

In this section, we review essential results concerning (i) the reconstruction of vacuum metric perturbations from curvature scalars, (ii) the failure of a naive metric reconstruction in the presence of sources, and (iii) the no-string reconstruction scheme for point-particle sources. From a certain point, we will specialize to a Schwarzschild background, introducing a decomposition of the various fields into multipole modes but refraining from a further frequency-mode decomposition and instead remaining in the time domain. Our purpose here is to remind readers of the relevant theory, introduce notation, and set up the relevant technical background for the rest of the analysis.

We adopt the Kinnersley null tetrad $e^\alpha_{\boldsymbol{a}} = \{\ell^\alpha, n^\alpha, m^\alpha, \bar m^\alpha\}$ [see Eq. (A1)], where boldface roman indices run over $1, \ldots, 4$ and denote tetrad components: $A_{\boldsymbol{a}} \coloneqq e^\alpha_{\boldsymbol{a}} A_\alpha$. The legs $e^\alpha_{\boldsymbol{a}}$ are all mutually orthogonal, except $\ell^\alpha n_\alpha = -1$ and $m^\alpha \bar m_\alpha = 1$. An overbar denotes complex conjugation. (Covariant) directional derivatives along the tetrad legs are denoted $\boldsymbol{D}_\ell = \ell^\alpha \nabla_\alpha$, $\boldsymbol{D}_n = n^\alpha \nabla_\alpha$, $\boldsymbol{D}_m = m^\alpha \nabla_\alpha$, and $\boldsymbol{D}_{\bar m} = \bar m^\alpha \nabla_\alpha$ (corresponding to the more customary but less transparent $\boldsymbol{D}$, $\boldsymbol{\Delta}$, $\boldsymbol{\delta}$, and $\bar{\boldsymbol{\delta}}$, respectively).

A. Vacuum case

The reconstruction of vacuum metric perturbations from curvature scalars was first prescribed in Ref. [28], but we follow here the concise presentation by Wald [29]. In what follows, hatted sans serif symbols ($\hat{\mathsf{E}}, \hat{\mathsf{T}}, \ldots$) represent linear differential operators on tensors.

Suppose $h_{\alpha\beta}$ is a solution of the vacuum Einstein's equation linearized about the Kerr metric:

$$\hat{\mathsf{E}} h \coloneqq \delta G(h) = 0. \tag{1}$$

Here, $\delta G_{\mu\nu}$ is the linearized Einstein tensor, thought of as a differential operator $\hat{\mathsf{E}}$ acting on $h_{\alpha\beta}$, and we have omitted tensorial indices for brevity. To this perturbation there correspond Weyl curvature scalars $\Psi_0 \eqqcolon \Psi_+$ and $\varrho^{-4}\Psi_4 \eqqcolon \Psi_-$ [see Eq. (A3); $\varrho = -1/r$ for Schwarzschild]. $\Psi_\pm$ are derived from $h_{\alpha\beta}$ via

$$\hat{\mathsf{T}}_\pm h = \Psi_\pm, \tag{2}$$

where the operators $\hat{\mathsf{T}}_\pm$ are given explicitly in Eq. (A4). Let $\hat{\mathsf{S}}_\pm$ be the operators that take the linearized Einstein's equation into the Teukolsky equations with spins ± 2, respectively,

$$\hat{\mathsf{S}}_\pm \hat{\mathsf{E}} h = \hat{\mathsf{O}}_\pm \Psi_\pm, \tag{3}$$

where $\hat{\mathsf{O}}_\pm$ is the Teukolsky operator given in Eq. (A6) and $\hat{\mathsf{S}}_\pm$ can be read off the source side of the Teukolsky equation (A5); these operators are given explicitly in Eqs. (A9) and (A10). From (2) and (3), there follows the operator identity

$$\hat{\mathsf{S}}_\pm \hat{\mathsf{E}} = \hat{\mathsf{O}}_\pm \hat{\mathsf{T}}_\pm. \tag{4}$$

Now, let $\Phi_\pm$ be (any) solution of the *adjoint*[1] vacuum Teukolsky equation,

$$\hat{\mathsf{O}}^\dagger_\pm \Phi_\pm (= \hat{\mathsf{O}}_\mp \Phi_\pm) = 0. \tag{5}$$

Noting $\hat{\mathsf{E}}$ is self-adjoint ($\hat{\mathsf{E}} = \hat{\mathsf{E}}^\dagger$), we then have

$$\hat{\mathsf{E}} \hat{\mathsf{S}}^\dagger_\pm \Phi_\pm = (\hat{\mathsf{S}}_\pm \hat{\mathsf{E}})^\dagger \Phi_\pm = (\hat{\mathsf{O}}_\pm \hat{\mathsf{T}}_\pm)^\dagger \Phi_\pm = \hat{\mathsf{T}}^\dagger_\pm \hat{\mathsf{O}}^\dagger_\pm \Phi_\pm = 0, \tag{6}$$

where in the second equality we have used (4). Thus, $h^\pm \coloneqq \hat{\mathsf{S}}^\dagger_\pm \Phi_\pm$ are (complex-valued) solutions of the vacuum Einstein's equation. A real-valued reconstructed solution is given by

$$h^{\rm rec}_\pm \coloneqq {\rm Re} \hat{\mathsf{S}}^\dagger_\pm \Phi_\pm. \tag{7}$$

The explicit form of the reconstruction operator $\hat{\mathsf{S}}^\dagger_\pm$ is given in Eqs. (A12). It returns $h^{\rm rec}_+$ in an *ingoing* radiation gauge (IRG), and $h^{\rm rec}_-$ in an *outgoing* radiation gauge (ORG),

$$h^{{\rm rec}+}_{\mathbf{1}\beta} = 0 \quad ({\rm IRG}), \qquad h^{{\rm rec}-}_{\mathbf{2}\beta} = 0 \quad ({\rm ORG}), \tag{8}$$

with both perturbations being traceless.

For $h^{\rm rec}_+$ and $h^{\rm rec}_-$ to each reproduce the original perturbation h, we must have $\hat{\mathsf{T}}_\pm h^{\rm rec}_+ = \Psi_\pm$ and $\hat{\mathsf{T}}_\pm h^{\rm rec}_- = \Psi_\pm$, leading to

$$\hat{\mathsf{T}}_\pm {\rm Re} \hat{\mathsf{S}}^\dagger_+ \Phi_+ = \Psi_\pm \quad ({\rm IRG}), \tag{9}$$

$$\hat{\mathsf{T}}_\pm {\rm Re} \hat{\mathsf{S}}^\dagger_- \Phi_- = \Psi_\pm \quad ({\rm ORG}). \tag{10}$$

These are the fourth-order "inversion" equations. A Hertz potential Φ_+ satisfying both the adjoint Teukolsky equation (5) and either of the two inversion relations in (9) will reproduce h up to some perturbation Δh_+ that is in the kernel of $\hat{\mathsf{T}}_+$; and a Hertz potential Φ_- satisfying both (5) and either of the two inversion relations in (10) will reproduce h up to some perturbation Δh_- that is in the kernel of $\hat{\mathsf{T}}_-$. That is,

$$h = h^{\rm rec}_\pm + \Delta h_\pm, \tag{11}$$

where

$$\hat{\mathsf{T}}_\pm \Delta h_\pm = 0. \tag{12}$$

---

[1] For a linear operator $\hat{\mathsf{L}}$ taking an n-rank tensor field ϕ to an m-rank tensor field ψ, the adjoint $\hat{\mathsf{L}}^\dagger$ takes ψ to ϕ and satisfies $(\hat{\mathsf{L}}^\dagger \psi)\phi = \psi(\hat{\mathsf{L}}\phi)$ (up to a divergence of an arbitrary vector field).

Wald [30] explored the kernel of $\hat{\mathsf{T}}_\pm$, and hence the space of $\Delta h_\pm$, for vacuum perturbations in Kerr. He found that $\Delta h_\pm$ is spanned by pure gauge perturbations (which are also in the kernel of $\hat{\mathsf{E}}$), in addition to exactly four types of stationary and axially symmetric (algebraically special) vacuum perturbations: a mass perturbation, an angular-momentum perturbation, and perturbations away from Kerr into the Kerr-NUT or the C-metric solutions.

B. Naive reconstruction with sources and its failure

The above procedure returns a solution to the *vacuum* linearized Einstein's equation (1). One may naively attempt to generalize this method to the nonvacuum case as follows. Suppose we wish to reconstruct a solution to

$$(\hat{\mathsf{E}}h)_{\alpha\beta} = 8\pi T_{\alpha\beta}, \tag{13}$$

where $T_{\alpha\beta}$ is some (first-order, perturbative) source of stress energy. It is tempting to try a Hertz potential that satisfies a sourced equation of the form

$$\hat{\mathsf{O}}^\dagger_\pm \Phi_\pm = S_\pm, \tag{14}$$

in lieu of the vacuum equation (5). Here, the source $S_\pm$ is to be determined from the condition that a metric perturbation reconstructed via (7) is a solution to (13). By operating on both sides of (14) with $\hat{\mathsf{T}}^\dagger_\pm$ [the adjoint of the operator $\hat{\mathsf{T}}$ in (2)] and then using the adjoint of the operator identity (4), one obtains the condition

$$\mathsf{T}^{\rm rec}_{\alpha\beta\pm} \coloneqq {\rm Re}(\hat{\mathsf{T}}^\dagger_\pm S_\pm)_{\alpha\beta} = 8\pi T_{\alpha\beta}. \tag{15}$$

However, considering the form of the operators $\hat{\mathsf{T}}^\dagger_\pm$ in Eqs. (A14) and (A15), we immediately see that (15) has no solutions for $S_\pm$, in general. For instance, observe that $T^{\rm rec}_{\alpha\beta\pm}$ is traceless, while $T_{\alpha\beta}$ need not be (and never is, in the case of a mass particle source, of interest to us here). Also observe that the tetrad components $T^{\rm rec}_{\mathbf{1}\beta+}$, $T^{\rm rec}_{\mathbf{2}\beta-}$, and $T^{\rm rec}_{\mathbf{34}\pm}$ all vanish identically, while the corresponding tetrad components of $T_{\alpha\beta}$ need not be zero. Thus, in general, our naive reconstruction procedure fails in nonvacuum regions of spacetime.

In recent work [31], Green *et al.* prescribed a modification of the above naive approach, based on adding a certain "corrector tensor" in Eq. (15) (together with a "completion" piece $\Delta h_\pm$), essentially to the effect of balancing out the component content of the two sides of the equation. They showed how, remarkably, the corrector can be obtained by integrating a certain hierarchical set of *ordinary* differential equations (ODEs) along null directions. There is ongoing work to demonstrate the applicability of this method in practice.

C. Point-particle source

A more acute question is whether the standard vacuum reconstruction procedure works in vacuum regions of spacetime in the presence of sources elsewhere. It has long been known, from analysis of the point-particle source example [32], that this was not the case; a perturbation $h^{\rm rec}_\pm$ reconstructed as in Eq. (7) (with or without a completion piece $\Delta h_\pm$) develops singularities in the vacuum region *away* from the particle. This can be appreciated already from the simple example of a static particle in flat space—see Sec. V C. of Ref. [32] or the more detailed analysis in Sec. VI of Ref. [22]. What one finds is that $h^{\rm rec}_\pm$ exhibits stringlike singularities that emanate from the particle along radial null directions. By adjusting the residual gauge freedom (within the class of radiation gauges), one can arrange to confine the string to either outgoing or ingoing directions, but no choice of a radiation gauge can rid of the strings altogether. The leading-order singular form of the string is described in Table I of Ref. [22]. The singularly is sufficiently strong that the perturbation field fails to be (absolutely) integrable over a two-dimensional surface intersecting the string, with the result that a multipole decomposition of the field is not even well defined. Thus, a mode-by-mode reconstruction procedure cannot work in the entire vacuum part of spacetime containing the string. It should be presumed that an analysis based on the new corrector-tensor method of Ref. [31] would reproduce this basic picture when applied to the point-particle case.

Let us describe the situation more precisely, using some new notation that will serve us through the rest of this work. We are interested in the case of a pointlike particle of mass μ, moving outside a Kerr black hole (to be specialized to Schwarzschild further below) with mass $M \gg \mu$. We assume the particle's stress energy is given by the distribution

$$T_{\alpha\beta} = \mu \int_{-\infty}^{\infty} u_\alpha u_\beta \delta^4(x^\alpha - x^\alpha_p(\tau))(-g)^{-1/2} d\tau, \tag{16}$$

where $x^\alpha_p(\tau)$ describes the particle's timelike worldline (τ being proper time), $u^\alpha \coloneqq dx^\alpha_p/d\tau$, and, as usual, indices are lowered using the background metric $g_{\alpha\beta}$ with determinant g. In Boyer-Lindquist coordinates (and a slight notational abuse), we write $x^\alpha_p(t) = (t, R(t), \theta_p(t), \varphi_p(t))$, so that $R(t)$ is the radial location of the particle at time t. We denote by $\mathcal{S}$ the $2+1$-dimensional closed surface $r = R(t)$; this is a 2-sphere through the particle at each given time. The surface $\mathcal{S}$ splits the exterior of the black hole into two disjoint regions, $r > R(t)$ and $r < R(t)$, which we call $\mathcal{S}^>$ and $\mathcal{S}^<$, respectively.

As we have described, a reconstructed radiation-gauge metric $h^{\rm rec}_\pm$ generically exhibits a string singularity in both $\mathcal{S}^>$ and $\mathcal{S}^<$: it is a "full-string" solution, in the terminology of Ref. [22]. It is not known how to calculate the physical self-force in such a pathological gauge, so the full-string reconstruction is not useful in the present context. As also described, there is a way to choose a radiation gauge such that the string is confined to $\mathcal{S}^>$ and the reconstructed perturbation, denoted here $h^<_\pm$, is regular (smooth) anywhere in $\mathcal{S}^<$. Similarly, there is a choice of radiation gauge for which the string is confined to $\mathcal{S}^<$, and the perturbation, denoted $h^>_\pm$, is regular (smooth) anywhere in $\mathcal{S}^>$. These are the two "half-string" solutions. Reference [22] showed how the physical self-force may be computed from either of the two half-string solutions using a procedure that involves taking a directional (radial) limit to the particle from its "regular" side. This procedure may be suitable for frequency-domain calculations, where one could (in principle) integrate the relevant radial ODE from boundary conditions either on the event horizon or at infinity, toward the particle, working in the regular side of spacetime. However, the half-string reconstructions are not suitable for time-domain calculations, where one evolves the field equations as partial differential equations (PDEs) on the full exterior of the black hole.

This brings us to the no-string reconstruction, first advocated in a series of papers by Friedman and collaborators [33–35] and later formulated in detail (and received its name) in Ref. [22]. The idea is simple: take the two regular sides of the two one-string solutions and glue them together at $\mathcal{S}$. The resulting, no-string perturbation is given by

$$h^{\rm nos}_\pm = h^<_\pm \Theta(R(t) - r) + h^>_\pm \Theta(r - R(t)), \tag{17}$$

where $\Theta(\cdot)$ is the Heaviside step function. The perturbation $h^{\rm nos}_\pm$ is regular (smooth) in both $\mathcal{S}^<$ and $\mathcal{S}^>$, where it solves the linearised vacuum Einstein's equations. On $\mathcal{S}$ itself, $h^{\rm nos}_\pm$ is not a vacuum solution, even away from the particle and even when allowing arbitrary completion pieces $\Delta h_{\alpha\beta}$ in and out of $\mathcal{S}$ [see Sec. VI.B.1 of Ref. [22], where it is shown that, at least in the flat-space example, the completed no-string solution differs from a vacuum solution by a singular perturbation with a distributional support (a delta function) on $\mathcal{S}$]. However, this failure of the no-string solution to be regular—or even a valid solution—on $\mathcal{S}$ turns out to be inconsequential in practice. Reference [22] obtained a formulation of the physical self-force, complete with a practical mode-sum formula, from a no-string metric perturbation. This formulation requires information about the perturbation field (and its derivatives) only in the one-sided radial limits $r \to R(t)^\pm$, which avoid $\mathcal{S}$. It is this formulation that forms the basis for Ref. [16]'s calculation of the gravitational self-force for generic orbits in Kerr spacetime, using a frequency-domain method.

Importantly for us here, the no-string reconstruction also, in principle, enables calculations in the time domain. The idea is to solve the relevant evolution equation in each of the two vacuum regions $\mathcal{S}^<$ and $\mathcal{S}^>$, with suitable jump conditions across $\mathcal{S}$. In our method, we solve directly for the Hertz potential in the two vacuum regions—$\Phi^<_\pm$ in $\mathcal{S}^<$ and $\Phi^>_\pm$ in $\mathcal{S}^>$—with suitable jump conditions that relate between $\Phi^<_\pm$ and $\Phi^>_\pm$ on $\mathcal{S}$. The key ingredient in this formulation is, indeed, the particular jumps necessary for $\Phi^\gtrless_\pm$ to reproduce the no-string perturbation via

$$h^\gtrless_\pm \coloneqq {\rm Re}\hat{\mathcal{S}}^\dagger_\pm \Phi^\gtrless_\pm. \tag{18}$$

The derivation of the required jumps, for generic geodesic orbits in a Schwarzschild geometry, will be described in Sec. IV.

First, however, we present a formulation of the evolution problem for $\Phi^\gtrless_\pm$ via a $1 + 1$-dimensional ($1 + 1$D) decomposition, henceforth specializing to the Schwarzschild case.

III. 1 + 1D EVOLUTION SCHEME FOR THE NO-STRING HERTZ POTENTIAL

A. Multipole decomposition

We recall the IRG fields $\Phi^\gtrless_+$ and ORG fields $\Phi^\gtrless_-$ have spin weights $s = -2$ and $s = +2$, respectively. We thus expand $\Phi^\gtrless_\pm$ in $s = \mp 2$ spin-weighted spherical harmonics,

$$\Phi_\pm = \frac{\Delta^{\pm 2}}{r} \sum_{\ell=2}^{\infty} \sum_{m=-\ell}^{\ell} \phi^{\ell m}_\pm(t, r)\, {}_{\mp 2}Y_{\ell m}(\theta, \varphi), \tag{19}$$

where for the time being we omit the labels $\gtrless$ for brevity. The normalization factor $\Delta^{\pm 2}/r$, where $\Delta \coloneqq r(r - 2M)$, is introduced (following Ref. [23]) to regulate the behavior of the time-radial fields $\phi^{\ell m}_\pm$ at infinity and on the horizon: it is such that the physical solutions (satisfying physical boundary solutions) generally approach constant nonzero values at both ends. The spherical basis functions ${}_{\mp 2}Y_{\ell m}$ can be derived from standard spherical harmonics $Y_{\ell m}(\theta, \varphi)$ via

$${}_{\pm 2}Y_{\ell m} = \sqrt{\frac{(\ell - 2)!}{(\ell + 2)!}} \left[\frac{\partial^2 Y_{\ell m}}{\partial \theta^2} - \left(\frac{\cos\theta \pm 2m}{\sin\theta} \right) \frac{\partial Y_{\ell m}}{\partial \theta} + \left(\frac{m^2 \pm 2m\cos\theta}{\sin^2\theta} \right) Y_{\ell m} \right]. \tag{20}$$

They satisfy the differential equation

$$\frac{1}{\sin\theta} \frac{\partial}{\partial\theta} \left(\sin\theta \frac{\partial_s Y_{\ell m}}{\partial\theta} \right) + \left(-\frac{m^2 + 2ms\cos\theta}{\sin^2\theta} - s^2\cot^2\theta + s + (\ell - s)(\ell + s + 1) \right) {}_sY_{\ell m} = 0, \tag{21}$$

and the symmetry relation

$${}_{\pm 2}\bar{Y}_{\ell m} = (-1)^m\, {}_{\mp 2}Y_{\ell,-m}. \tag{22}$$

We also note the symmetry under reflection by the equatorial plane,

$$ {}_{\pm2}Y_{\ell m}(\theta,\varphi) = (-1)^{\ell}\,{}_{\pm2}\bar{Y}_{\ell,-m}(\pi-\theta,\varphi), \tag{23}$$

to become useful further below.

For our derivation of the jump conditions across $\mathcal{S}$ (in Sec. IV below), we will also need a decomposition of the Weyl scalars in the same basis. Recalling $\Psi_{\pm}$ have spin weights $s=\pm2$, we introduce

$$\Psi_{\pm} = \frac{\Delta^{\mp2}}{r}\sum_{\ell=2}^{\infty}\sum_{m=-\ell}^{\ell}\psi_{\pm}^{\ell m}(t,r)\,{}_{\pm2}Y_{\ell m}(\theta,\varphi). \tag{24}$$

In what follows, we frequently drop the labels ℓ, m off of $\phi_{\pm}^{\ell m}$ and $\psi_{\pm}^{\ell m}$ for notational economy; it should be remembered that Φ and Ψ are the full four-dimensional fields, while ϕ and ψ are the corresponding $1+1\mathrm{D}$ reductions.

B. Bardeen-Press-Teukolsky equation in 1+1D

With the substitution (19), the adjoint vacuum BPT equation (5) separates into ℓ, m modes, with each modal function $\phi_{\pm}(t,r)$ satisfying the $1+1\mathrm{D}$ wave equation

$$\phi^{\pm}_{,uv} + U_s(r)\phi^{\pm}_{,u} + V_s(r)\phi^{\pm}_{,v} + W_s(r)\phi^{\pm} = 0, \tag{25}$$

with $s=\mp2$ for $\phi_{\pm}$. Here,

$$U_s(r) = -\frac{sM}{r^2}, \qquad V_s(r) = \frac{sf}{r}, \tag{26}$$

$$W_s(r) = \frac{f}{4}\left(\frac{(\ell+s+1)(\ell-s)}{r^2} + \frac{2(1+s)M}{r^3}\right), \tag{27}$$

with

$$f \coloneqq 1 - 2M/r = \Delta/r^2. \tag{28}$$

We have introduced here the Eddington-Finkelstein null coordinates $v = t + r_*$ and $u = t - r_*$, where $r_* = r + 2M\ln[r/(2M) - 1]$. Our convention is that, when acting on a function of u and v, ∂_u and ∂_v are always taken with fixed v and fixed u, respectively.

Similarly, in vacuum, the modal functions $\psi_{\pm}(t,r)$ of the Weyl scalars satisfy the $1+1\mathrm{D}$ BPT equations

$$\psi^{\pm}_{,uv} + U_s(r)\psi^{\pm}_{,u} + V_s(r)\psi^{\pm}_{,v} + W_s(r)\psi_{\pm} = 0, \tag{29}$$

with $s=\pm2$ for $\psi_{\pm}$.

C. Inversion relations in 1+1 dimensions

In our method, we solve for the (modal) Hertz potential ϕ directly, making use of neither the BPT equation (29) for ψ, nor the inversion relations that link ψ to ϕ. However, we *will* make use of the inversion relations in deriving jump conditions for ϕ across $\mathcal{S}$ (this will be done in Sec. IV), and for that purpose, we need these relations in a $1+1\mathrm{D}$ form.

The inversion relations for Φ_+ and Φ_- were given in Eqs. (9) and (10), respectively. We recall there are two alternative relations for each of the two gauges, one linking (each of) $\Phi_{\pm}$ to Ψ_+ and another linking them to Ψ_-. In the Schwarzschild case, the relations read

$$\boldsymbol{D}_{\ell}^4\bar{\Phi}_+ = 2\Psi_+, \tag{30a}$$

$$\Delta^2\tilde{\boldsymbol{D}}_n^4\Delta^2\bar{\Phi}_- = 32\Psi_- \tag{30b}$$

("radial" inversion) and

$$\bar{\eth}_{-1}\bar{\eth}_0\bar{\eth}_1\bar{\eth}_2\bar{\Phi}_+ - 12M\partial_t\Phi_+ = 8\Psi_-, \tag{31a}$$

$$\eth_1\eth_0\eth_{-1}\eth_{-2}\bar{\Phi}_- + 12M\partial_t\Phi_- = 8\Psi_+ \tag{31b}$$

("angular" inversion). The differential operators $\boldsymbol{D}_{\ell}$ and $\tilde{\boldsymbol{D}}_n$, whose general definition is given just below Eq. (A6), are, in the Schwarzschild case,

$$\boldsymbol{D}_{\ell} = (2/f)\partial_v, \qquad \tilde{\boldsymbol{D}}_n = -(2/f)\partial_u. \tag{32}$$

The operators $\eth_s$ and $\bar{\eth}_s$ are the "spin raising" and "spin lowering" angular operators defined in Eq. (A7), whose action on ${}_sY_{\ell m}(\theta,\varphi)$ is described in Eq. (A8).

To separate the radial inversion relations (30) into multipole modes, we first take the complex conjugate of (19) to obtain

$$\bar{\Phi}_{\pm} = \frac{\Delta^{\pm2}}{r}\sum_{\ell,m}\bar{\phi}_{\pm}^{\ell,-m}(-1)^m\,{}_{\pm2}Y_{\ell m}, \tag{33}$$

where use was made of the symmetry relation (22). The expansions (33) and (24) then separate Eqs. (30) to give, for each ℓ, m, the fourth-order ODEs

$$r\Delta^2\boldsymbol{D}_{\ell}^4(\Delta^2\phi_+^{\ell m}/r) = 2(-1)^m\bar{\psi}_+^{\ell,-m}, \tag{34a}$$

$$r\tilde{\boldsymbol{D}}_n^4(\phi_-^{\ell m}/r) = 32(-1)^m\bar{\psi}_-^{\ell,-m}. \tag{34b}$$

These relations can be written in a tidier form when the perturbation possesses a symmetry of refection about the equatorial plane, as in the setup to be considered in this paper: a particle source moving in the equatorial plane of the Schwarzschild black hole. In this case, we have the symmetry relation

$$\bar{\psi}_{\pm}^{\ell,-m} = (-1)^{\ell}\psi_{\pm}^{\ell m}, \tag{35}$$

which follows from the following argument. First, we note that under the reflection transformation $\theta \to \pi - \theta$ (with fixed t, r, φ) the tetrad legs ℓ^{α} and n^{α} remain invariant, while $m^{\alpha} \to -\bar{m}^{\alpha}$ and $\bar{m}^{\alpha} \to -m^{\alpha}$ [see Eqs. (A1)].

Inspecting Eqs. (A3), we see this implies $\Psi_\pm \to \bar{\Psi}_\pm$, assuming the perturbed Weyl tensor $C_{\alpha\beta\gamma\delta}$ is invariant under such reflection. Thus, using (23), we have

$$\begin{aligned}\Psi_\pm(\theta) = \bar{\Psi}_\pm(\pi-\theta) &= \frac{\Delta^{\mp 2}}{r}\sum_{\ell,m}\bar{\psi}_\pm^{\ell m}\,{}_{\pm 2}\bar{Y}_{\ell m}(\pi-\theta)\\ &= \frac{\Delta^{\mp 2}}{r}\sum_{\ell,m}\bar{\psi}_\pm^{\ell,-m}(-1)^\ell\,{}_{\pm 2}Y_{\ell m}(\theta),\end{aligned} \tag{36}$$

and a comparison with (24) then leads to (35). Using (35), we now write the 1 + 1D radial inversion relations (34) in their final form,

$$r\Delta^2 \boldsymbol{D}_\ell^4(\Delta^2\phi_+^{\ell m}/r) = 2p\psi_+^{\ell m}, \tag{37a}$$

$$r\tilde{\boldsymbol{D}}_n^4(\phi_-^{\ell m}/r) = 32p\psi_-^{\ell m}, \tag{37b}$$

where

$$p \coloneqq (-1)^{\ell+m} \tag{38}$$

is the "parity" factor. We note (37) implies the 1 + 1D Hertz potentials share the same refection symmetry as the 1 + 1D Weyl scalars[2]:

$$\bar{\phi}_\pm^{\ell,-m} = (-1)^\ell \phi_\pm^{\ell m}. \tag{39}$$

Let us next separate the angular inversion formulas (31). Using (A8) with (33) and (39), we have

$$\bar{\eth}_{-1}\bar{\eth}_0\bar{\eth}_1\bar{\eth}_2\bar{\Phi}_+ = \frac{\Delta^2}{r}\sum_{\ell,m}p\lambda_2\phi_+^{\ell m}\,{}_{-2}Y_{\ell m}, \tag{40a}$$

$$\eth_1\eth_0\eth_{-1}\eth_{-2}\bar{\Phi}_- = \frac{\Delta^{-2}}{r}\sum_{\ell,m}p\lambda_2\phi_-^{\ell m}\,{}_{+2}Y_{\ell m}, \tag{40b}$$

where

$$\lambda_n \coloneqq \frac{(\ell+n)!}{(\ell-n)!}. \tag{41}$$

With this substitution, Eqs. (31) separate to give, for each ℓ, m, the first-order ODEs

$$\partial_t\phi_\pm^{\ell m} \mp p\alpha\phi_\pm^{\ell m} = \mp\frac{2}{3M}\psi_\mp^{\ell m}, \tag{42}$$

where

$$\alpha = \frac{\lambda_2}{12M}. \tag{43}$$

We note that it is obviously possible to solve (42) in closed form in terms of a time integral involving $\psi_\mp$ (this was the main result of Ref. [36]). That, however, would not serve our purpose here. Recall that the inversion relations (42) are only valid in vacuum and cannot be used (despite temptation) to relate the distributional contents of $\psi_\mp$ on $\mathcal{S}$ to these of the no-string Hertz potentials $\phi_\pm$. The idea, instead, is to use the inversion relations *evaluated in the two vacuum domains* $\mathcal{S}^>$ and $\mathcal{S}^<$ in order to get information about the jumps in $\phi_\pm$ across $\mathcal{S}$, given the known jumps in $\psi_\mp$. As we show in the next section, with some further manipulation [which also involves the radial inversion relations (37)], this procedure can completely determine the jumps in $\phi_\pm$ and all of their derivatives on $\mathcal{S}$.[3]

We also note the relation (42) means that (given $\psi_\mp$) all time derivatives of $\phi_\pm$ are determinable *algebraically* from $\phi_\pm$ itself. For example, taking ∂_t of (42) and then substituting for $\partial_t\phi$ back from Eq. (42), we find

$$\partial_{tt}\phi_\pm = \alpha^2\phi_\pm \mp \frac{2}{3M}(\partial_t\psi_\mp \pm p\alpha\psi_\mp). \tag{44}$$

Taking ∂_r of (42) similarly determines $\partial_{tr}\phi_\pm$ algebraically from $\phi_\pm$ and $\partial_r\phi_\pm$. With the help of the vacuum BPT equation (25), we can then iteratively express $\partial_{rr}\phi_\pm$ and all higher derivatives of $\phi_\pm$ algebraically in terms of $\phi_\pm$ and $\partial_r\phi_\pm$ alone. The significance of this in the context of this work is as follows: it means we need only to determine the jumps across $\mathcal{S}$ of $\phi_\pm$ and of its first r derivative; the jumps in all t, r, and mixed derivatives to all orders are obtainable algebraically from these two alone.

D. Initial/boundary-value formulation

Our strategy is to solve the 1 + 1D vacuum hyperbolic equation (25) directly as a time evolution problem from initial data outside the black hole. The fields $\phi_+^{\gtrless}$ are to be evolved on the respective vacuum domains $\mathcal{S}^{\gtrless}$, with suitable jump conditions imposed on the timelike interface $\mathcal{S}$ (cf. Fig. 1 for an illustration of this setup with characteristic initial data). In principle, it suffices to impose the jumps in the field and in its first normal derivative at $\mathcal{S}$. The solution is then uniquely determined once boundary conditions are imposed at null infinity (past or future, $\mathcal{I}^\pm$) and on the event horizon (past or future, $\mathcal{H}^\pm$).

The specific form of boundary conditions for $\phi_+^{\gtrless}$ is inherited from that of the reconstructed no-string

---

[2] More precisely, Eqs. (37) alone imply (39) only up to homogeneous solutions of (37). However, no homogeneous solution of (37) satisfies the BPT equations as required, so such solutions can be excluded.

[3] Here, we use $\mathcal{S}$ to represent the curve $r = R(t)$ in the r, t plane, while in Sec. II it was introduced as the 2 + 1D sphere $r = R(t)$ in spacetime. Throughout this work, we will continue to use $\mathcal{S}$ in both ways; the relevant meaning in each instance should be clear from the context. A similar remark applies to $\mathcal{S}^<$ and $\mathcal{S}^>$.

metric $h_{\pm}^{\rm rec}$. For the applications we have in mind (e.g., a self-force calculation), it is the *retarded* (hereafter "physical") perturbation that we are after, i.e., the one corresponding to the boundary conditions of having no radiation coming in from $\mathcal{I}^-$ or out of $\mathcal{H}^-$. These requirements can be translated into asymptotic conditions on the behavior of $\phi_{\pm}^{>}$ at infinity and of $\phi_{\pm}^{<}$ on the horizon (we are assuming here an orbit that does not plunge into the black hole, so that $\mathcal{S}$ does not cross the horizon). This analysis was carried out in Ref. [23], and we quote the results here. For a monochromatic physical perturbation that has the asymptotic form approximately $e^{-i\omega u}/r$ at $\mathcal{I}^+$ (in a suitable Lorentzian frame) and $e^{-i\omega v}$ on $\mathcal{H}^+$ (in a suitable horizon-regular frame), for some frequency $\omega > 0$, the corresponding Hertz potential modes admit

$$\begin{aligned} \phi_{\pm}^{>}(r\to\infty) &\sim e^{-i\omega u} \qquad \text{(physical)},\\ \phi_{\pm}^{<}(r\to 2M) &\sim e^{-i\omega v} \qquad \text{(physical)}. \end{aligned} \tag{45}$$

Note $\phi_{\pm}$ generically approach constant nonzero values at $\mathcal{I}^+$ ($r\to\infty$ with constant u) and on the $\mathcal{H}^+$ ($r\to 2M$ with constant v). To achieve this convenient behavior was the purpose of introducing the radial prefactors in Eq. (33).

For the interpretation of numerical results in Sec. V, it will be useful to also have at hand the asymptotic behavior of "nonphysical" monochromatic modes, which correspond to waves coming in from $\mathcal{I}^-$, $h_{\pm}^{\rm rec}\sim e^{-i\omega v}/r$, or to waves coming out of $\mathcal{H}^-$, $h_{\pm}^{\rm rec}\sim e^{-i\omega u}$. For such solutions, the asymptotic analysis in Ref. [23] finds

$$\begin{aligned} \phi_{\pm}^{>}(r\to\infty) &\sim r^{\mp 4}e^{-i\omega v} \qquad \text{(nonphysical)},\\ \phi_{\pm}^{<}(r\to 2M) &\sim \Delta^{\mp 2}e^{-i\omega u} \qquad \text{(nonphysical)}. \end{aligned} \tag{46}$$

The main missing ingredient in the above formulation is the jump conditions across $\mathcal{S}$. We proceed, in the next section, with a derivation of these conditions for generic geodesic orbits.

IV. JUMP CONDITIONS FOR THE NO-STRING HERTZ POTENTIAL

Reference [23] sketched a method for obtaining the jumps across $\mathcal{S}$ for a generic geodesic orbit in Kerr spacetime, but the actual jumps were only calculated for circular orbits in the Schwarzschild case. In the general case (and even in the Schwarzschild limit), the method requires the solution of a complicated set of coupled fourth-order ODEs for the jumps in ϕ and in $\phi_{,r}$ along the orbit. There was no attempt to solve these equations (neither analytically nor numerically), except in the circular-orbit case, where they reduce to algebraic equations.

Here, we describe a different method for obtaining the jumps and apply it to generic orbits in the Schwarzschild case. The method yields a single first-order ODE for the jump in ϕ along the orbit, which can be solved in closed form. The jumps in all partial derivatives of ϕ, at any order, are then obtained algebraically from that solution. There were two key advances that made possible this much simpler and more effective approach: first, we have found a way of utilizing both radial and angular inversion formulas in tandem, in a particular way that simplifies the calculation. Second, we have observed certain algebraic simplifications that were overlooked (by one of us) in Ref. [23].

We consider here only the IRG Hertz potential Φ_+ (as also in Ref. [23]), but the jumps for the ORG potential Φ_- can be worked out in just the same way. We henceforth omit the label $+$ for notational economy, taking $\Phi\equiv\Phi_+$ and $\phi^{\ell m}(t,r)\equiv\phi_+^{\ell m}(t,r)$. We let the interface $\mathcal{S}$ be described by the smooth function $r=R(t)$ and denote the jump in $\phi(t,r)$ across $\mathcal{S}$ by

$$[\phi] \coloneqq \lim_{\epsilon\to 0}[\phi^{>}(t,R(t)+\epsilon)-\phi^{<}(t,R(t)-\epsilon)]. \tag{47}$$

The jumps in other $1+1$D fields are similarly defined: $[\phi_{,r}]$, $[\phi_{,t}]$, $[\psi_{\pm}]$, etc. We think of $[\phi]$ as a function of coordinate time t along the orbit and note the relation

$$\dot{[\phi]} = [\phi_{,t}] + \dot{R}[\phi_{,r}], \tag{48}$$

where an overdot denotes d/dt.

In what follows, we assume that the jumps across $\mathcal{S}$ of the modal Weyl scalars $\psi_{\pm}^{\ell m}(t,r)$ and of their first three derivatives are already known and are given. These jumps can be obtained in a straightforward way from the source of the Teukolsky equation. We carry out this calculation in Appendix B for generic (geodesic) orbits and for both ψ_- and ψ_+ (as both will be needed in our approach even if we restrict to the IRG potential ϕ_+).

A. Expressions for $[\phi_{,t}]$ and $[\phi_{,r}]$ in terms of $[\phi]$

Our task is to express each of $[\phi_{,r}]$ and $[\phi_{,t}]$ in terms of $[\phi]$ alone (and possibly the known jumps in the Weyl scalars). Substitution in (48) would then give a first-order ODE for $[\phi]$. The second half of this task can be accomplished immediately thanks to the angular inversion formula (42). We obtain

$$[\phi_{,t}] = p\alpha[\phi] - \frac{2}{3M}[\psi_-]. \tag{49}$$

The jump $[\psi_-]$ is given in Eq. (B17) of Appendix B, and recall $\alpha=\lambda_2/(12M)$. To obtain $[\phi_{,r}^{(\pm)}]$ in terms of $[\phi]$ is harder and utilizes the fourth-order radial inversion (37), using a procedure we now describe.

First, we write (37a) more explicitly in terms of coordinate derivatives. Using $\boldsymbol{D}_\ell = 2(r^2/\Delta)\partial_v$ (taken with fixed u), a calculation yields

$$\partial_v^4\phi + \frac{2}{r^2}(3r-5M)\partial_v^3\phi + \frac{1}{r^4}(9r^2-26Mr+15M^2)\partial_v^2\phi + \frac{1}{2r^5}(6r^2-21Mr+16M^2)\partial_v\phi = \frac{p}{8r^8}\psi_+. \tag{50}$$

We now act with ∂_u (fixed v) on both sides of (50) and use the vacuum BPT equation (25) to substitute for each mixed derivative $\phi_{,uv}$ in terms of $\phi_{,u}$, $\phi_{,v}$, and ϕ. In the resulting expression, we then substitute for $\partial_v^4\phi$ from Eq. (50). We arrive at a third-order ODE of the form

$$\sum_{n=0}^{3}\hat{A}_n(r)\partial_v^n\phi = \sum_{n=0}^{1}\hat{B}_n(r)\partial_u^n\psi_+, \tag{51}$$

where $\hat{A}_n(r)$ and $\hat{B}_n(r)$ are certain (rational) functions. Notably, no u derivatives occur on the lhs. Repeating this procedure with a second application of ∂_u, this time replacing $\partial_v^3\phi$ from Eq. (51), yields a second-order ODE of the form

$$\sum_{n=0}^{2}\tilde{A}_n(r)\partial_v^n\phi = \sum_{n=0}^{2}\tilde{B}_n(r)\partial_u^n\psi_+, \tag{52}$$

with some other (rational) functions $\tilde{A}_n(r)$ and $\tilde{B}_n(r)$. Again, we find that no u derivatives occur on the lhs. One last application of ∂_u reduces the inversion relation to a first-order differential equation, which, however, is now a PDE, since (it turns out) it features both $\phi_{,u}$ and $\phi_{,v}$. We can, however, reduce this to an ODE by first converting to r_* and t derivatives using $\phi_{,v} = \frac{1}{2}(\phi_{,t}+\phi_{,r_*})$ and $\phi_{,u} = \frac{1}{2}(\phi_{,t}-\phi_{,r_*})$, and then eliminating $\phi_{,t}$ using the angular inversion relation (42). This leads to a first-order ODE for ϕ, which has the form

$$\phi_{,r_*} + A(r)\phi = p\sum_{n=0}^{3}B_n(r)\partial_u^n\psi_+ + B(r)\psi_-. \tag{53}$$

An explicit calculation gives

$$A(r) = -\alpha + \frac{2M[(2\lambda_1-3)r-6M]}{r^2(\lambda_1 r-6M)} \tag{54}$$

for odd-parity modes ($p=-1$) and

$$A(r) = \alpha + \frac{M[4r^3\alpha^2(2\lambda_1+3)+2r^2\alpha\lambda_1(\lambda_1+4)+\lambda_1^2(3r-2M)]}{r^2[2\alpha^2r^2(\lambda_1 r+6M)+M\lambda_1(6\alpha r+\lambda_1)]} \tag{55}$$

for even-parity modes ($p=+1$). The other radial coefficients in Eq. (53) are found to be given by

$$\begin{aligned}
B_0 &= \lambda_1 f^3 r(\lambda^2r^2+3M\lambda r+6M^2)/C(r),\\
B_1 &= [18\alpha\lambda Mr^4+8M^2r^3\alpha(9-7\lambda)+M^2r^2(4\lambda^3-9\lambda^2-31\lambda+24)+2M^3r(\lambda+3)(7\lambda-13)+12M^4(\lambda+5)]/C(r),\\
B_2 &= 12Mr^2[\alpha\lambda r^3-\alpha(\lambda-5)Mr^2+2(1-2M\alpha)Mr-4M^2]/C(r),\\
B_3 &= 4Mr^3[\alpha r^2(\lambda r+6M)+3Mrf]/C(r),\\
B &= -4f^3M^2r^2[6\alpha r^4(\alpha^2r^2+\lambda)-r^3\lambda(\lambda^2-4)+9Mr^2(1-6M\alpha)-36M^2(r-M)]/C(r),
\end{aligned} \tag{56}$$

with

$$C = 18M^3f^3r^4\alpha[-2\alpha^2r^4-\lambda r^2+2Mr(\lambda-1)+6M^2]. \tag{57}$$

Here, we have introduced

$$\lambda \coloneqq \lambda_2/\lambda_1 = (\ell+2)(\ell-1), \tag{58}$$

and we remind the reader that $\lambda_1 = \ell(\ell+1)$ and $\alpha = \lambda_2/(12M)$.

Using Eq. (53), we can finally express the jump $[\phi_{,r_*}] = f(R)[\phi_{,r}]$ in terms of the jump $[\phi]$ (and the known jumps in the Weyl scalars $\psi_\pm$):

$$[\phi_{,r_*}] = -A(R)[\phi] + p\sum_{n=0}^{3}B_n(R)[\partial_u^n\psi_+] + B(R)[\psi_-]. \tag{59}$$

B. First-order ODE for $[\phi]$ and its solution

Substituting (49) and (59) in (48) now gives a simple first-order ODE for $[\phi]$ as a function along the orbit,

$$[\dot{\phi}] + (A(R)\dot{R}_* - p\alpha)[\phi] = \mathcal{F}, \tag{60}$$

where $\dot{R}_* = \dot{R}/f(R)$. The source term here is

$$\mathcal{F}=p\dot{R}_*\sum_{n=0}^{3}B_n(R)[\partial_u^n\psi_+]+\left(\dot{R}_*B(R)-\frac{2}{3M}\right)[\psi_-]. \tag{61}$$

Equation (60) admits simple homogeneous solutions, given by (any constant multiple of)

$$[\phi]_h=\left(\frac{R(\lambda_1 R-6M)}{(R-2M)^2}\right)\times e^{-\alpha(t-R_*)} \tag{62}$$

for odd-parity modes or

$$[\phi]_h=\left(\frac{R^3\lambda^2\lambda_1+6MR^2\lambda^2+36M^2R\lambda+72M^3}{R(R-2M)^2}\right)\times e^{\alpha(t-R_*)} \tag{63}$$

for even-parity modes. The general inhomogeneous solution of (60) reads

$$[\phi]=[\phi]_h\int_{t_0}^{t}\frac{\mathcal{F}(t')}{[\phi]_h}dt', \tag{64}$$

where t_0 is an *a priori* arbitrary integration constant. We determine t_0 from the physical requirement that $[\phi]$ remains bounded for $t\to\pm\infty$. Observing that $[\phi]_h$ blows up like $e^{\pm\alpha t}$ at $t\to\pm\infty$ (+ for even parity modes and − for odd-parity modes), while $\mathcal{F}(t)$ is at worst polynomial in t, it is easy to see that the requirement of boundedness necessitates $t_0=\pm\infty$ for $p=\pm1$. Hence, the unique physical solution of (60) is

$$[\phi]=[\phi]_h\int_{\pm\infty}^{t}\frac{\mathcal{F}(t')}{[\phi]_h}dt' \quad (\text{for } p=\pm1). \tag{65}$$

Equation (65) gives the jumps across $\mathcal{S}$ that the no-string Hertz potential modes must satisfy, for an arbitrary orbit in Schwarzschild spacetime. (It requires as input the jumps in the modes of the Weyl scalars, which in Appendix B we give explicitly specialized to geodesic orbits, but given the Weyl scalar jumps, there is no further assumption on whether the orbit is geodesic.) This is one of the main results of this paper.

We recall that the jumps in the field's derivatives, $[\phi_{,t}]$ and $[\phi_{,r}]$ (or $[\phi_{r_*}]$), can be obtained algebraically from $[\phi]$, using Eqs. (49) and (59), respectively. In principle, knowledge of the jumps in the field and its first derivatives should suffice in our formulation. However, in practice, it is also useful to have at hand the jumps in higher derivative, which eases the formulation of finite-difference schemes that have high-order convergence properties. Once the jumps in the field and its first derivatives are known, it is straightforward to obtain the jumps in higher derivatives in an iterative manner using the procedure described in the last paragraph of Sec. III C [the paragraph containing Eq. (44)]. The application of this procedure up to third derivatives is illustrated in Appendix B 3 (as applied to modes of the Weyl scalars).

C. Large-*R* asymptotics for scatter orbits

We were not able to evaluate the integral in (65) analytically for a generic orbit, but it is straightforward to compute $[\phi](t)$ numerically for any given geodesic orbit. In practice, we find it easier to obtain $[\phi]$ by (numerically) solving the first-order ODE (60). For the class of scatter orbits of interest to us in this paper, we need to integrate the equation over $-\infty<t<\infty$. We choose to do so forward in time for odd-parity modes but backward in time for even-parity modes, in each case going “against" the direction of exponential growth of the homogeneous solutions (62) and (63). This prevents the growth of nonphysical modes from numerical error. We now derive the leading-order asymptotic form of $[\phi]$ at $t\to\pm\infty$. One of these two asymptotic values will be used as an initial value for the ODE solver, and the other will be used to check the result of the numerical integration.

We consider a timelike scatter geodesic orbit in Schwarzschild spacetime, parametrized by specific energy $E>1$ (“gamma factor”) and angular momentum L (a more detailed description of such orbits will be given in Sec. VII A below). We let

$$\dot{R}_\infty := \pm|\dot{R}(t\to\pm\infty)| = \pm\frac{\sqrt{E^2-1}}{E} \tag{66}$$

be the “velocity at infinity” (with respect to coordinate time t), so that $\dot{R}_\infty$ is negative (positive) for the inbound (outbound) asymptotic states. We formally expand $[\phi]$ as a power series in $1/R$ at large $R(t)$ and seek to obtain the leading term of that expansion.

To this end, we first obtain the large-R asymptotic form of $\mathcal{F}$ in Eq. (61). Using as input the asymptotic expressions derived in Appendix B 4 for $[\psi_-]$ and $[\partial_u^n\psi_+]$ $(n=0,\ldots,3)$, a direct calculation leads to

$$\mathcal{F}=c_0R^{-3}+O(R^{-4}), \tag{67}$$

where

$$\begin{aligned}c_0=\frac{4\pi\mu(1+\dot{R}_\infty)}{3\lambda_2}&[i(L/M)\lambda_2(\partial_\theta-m)\,{}_{-2}\bar{Y}_{\ell m}\\&+6E\dot{R}_\infty(\partial_{\theta\theta}-2m\partial_\theta+(m^2-2))\,{}_{-2}\bar{Y}_{\ell m}].\end{aligned} \tag{68}$$

Here, all angular functions are evaluated at $\theta=\pi/2$ and $\varphi=\varphi_{\rm in}$ (or $\varphi=\varphi_{\rm out}$), with $\varphi_{\rm in}$ ($\varphi_{\rm out}$) being the asymptotic value of the particle's azimuthal phase at $t\to-\infty$ $(t\to+\infty)$. Equation (68) takes a neater form when written in terms of spin-0 spherical harmonics. With the aid of (20), we find

$$c_0 = \frac{4\pi\mu(1+\dot{R}_\infty)}{3M\sqrt{\lambda_2}}[(6ME\dot{R}_\infty - im\lambda L)\bar{Y} - i\lambda L\bar{Y}_\theta], \qquad (69)$$

where $\bar{Y} \coloneqq \bar{Y}_{\ell m}(\frac{\pi}{2}, \varphi_{\mathrm{in/out}})$ and $\bar{Y}_\theta \coloneqq \partial_\theta \bar{Y}_{\ell m}(\frac{\pi}{2}, \varphi_{\mathrm{in/out}})$.

The asymptotic form of $[\phi]$ can now be obtained either by evaluating (65) with the asymptotic form (67) or directly from the ODE (60) using a power-law ansatz. Either way, we arrive at

$$[\phi]_{R\to\infty} = -\frac{16\pi\mu}{\lambda_2^{3/2}}\left(\frac{1+\dot{R}_\infty}{1-\dot{R}_\infty}\right)[6M\dot{R}_\infty E\bar{Y} \\ + i\lambda L(\bar{Y}_\theta - m\bar{Y})]R^{-3} + O(R^{-4}). \qquad (70)$$

We note $\bar{Y}_\theta = 0$ for even-parity modes and $\bar{Y} = 0$ for odd-parity modes. Our result (70) can be checked against the $m = 0$, circular-orbit expression given in Eq. (87) of Ref. [23], by setting $\dot{R}_\infty = 0$, $r_0 = R$, $\Omega = \sqrt{M/R^3}$ and $\mathcal{Y}_\theta = -\lambda\bar{Y}_\theta/\sqrt{\lambda_2}$. We find an agreement.

In Sec. VI, for reasons that will become clear there, we will require also the asymptotic forms of the jumps $[\phi_{,v}]$ and $[\phi_{,vv}]$. The jump $[\phi_{,v}] = \frac{1}{2}([\phi_{,t}] + [\phi_{,r_*}])$ is obtained using Eqs. (49) and (59) with the known asymptotic expressions for $[\phi]$, $[\psi_-]$ and $[\partial_u^n\psi_+]$. The result is

$$[\phi_{,v}]_{R\to\infty} = \frac{4\mu\pi E(1+\dot{R}_\infty)}{\sqrt{\lambda_2}}\bar{Y}R^{-3} + O(R^{-4}). \qquad (71)$$

The asymptotic form of $[\phi_{,u}]$ is obtained in a similar way. The jump $[\phi_{,vv}]$, in turn, can be written in terms of lower-derivative jumps as explained in the last paragraph of Sec. III C, and substituting the asymptotic expressions already obtained for these, one finds

$$[\phi_{,vv}]_{R\to\infty} = -\frac{4\mu\pi E(2+\dot{R}_\infty)}{\sqrt{\lambda_2}}\bar{Y}R^{-4} + O(R^{-5}). \qquad (72)$$

V. TIME-DOMAIN EVOLUTION OF THE TEUKOLSKY EQUATION: PROBLEM OF GROWING MODES

A. Numerical method

Our aim, in the remainder of this paper, is to demonstrate the applicability of our strategy with an end-to-end numerical implementation. First, in this section, we implement a simple finite-difference Teukolsky solver based on 1 + 1D characteristic evolution in u, v coordinates. The basic architecture of the code is similar to that of the one developed in Ref. [23], but our new code can handle any orbit (Ref. [23] had circular orbits hardwired into it) and can evolve both the IRG ($s = -2$) and the ORG ($s = +2$) Hertz potentials (Ref. [23] dealt only with $s = -2$). We have produced two identical implementations, one in *Mathematica* and another in C++, to enable cross-checks.

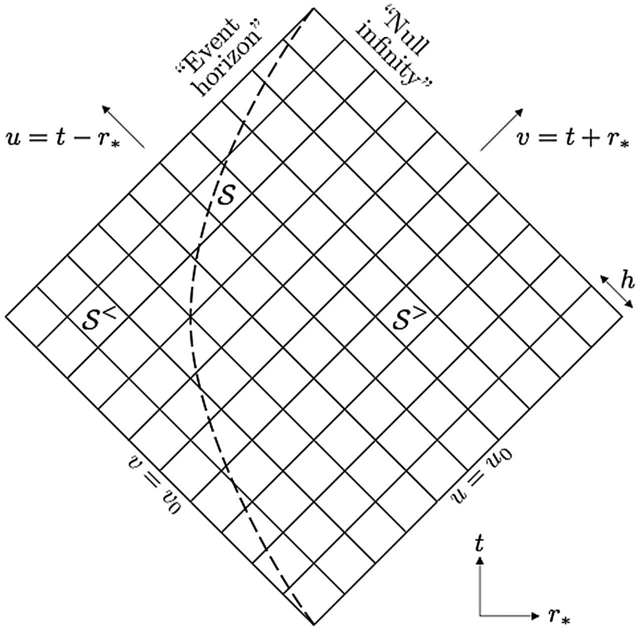

FIG. 1. Sketch of the 1 + 1D characteristic grid used in our numerical evolution of the no-string Hertz potentials $\phi_\pm^{\ell m}(t,r)$ outside a Schwarzschild black hole. The grid lines are uniformly spaced in Eddington-Finlkelstein coordinates u, v. Initial conditions are set on the rays $u = u_0$ and $v = v_0$. The dashed line represents the particle's worldline (or, equivalently, the 1 + 1D reduction of the surface $\mathcal{S}$ interfacing between the vacuum regions $\mathcal{S}^{\gtrless}$) for a typical hyperbolic orbit. The evolution proceeds along successive $u =$ const rays, with appropriate jump conditions imposed across $\mathcal{S}$.

The numerical domain is depicted in Fig. 1. We use a fixed characteristic mesh, with uniform grid-cell dimensions $h \times h$, where h is a small fraction of M (typically approximately $M/10$ to approximately $M/100$ in our test runs). Characteristic initial data are set on two initial rays $v = v_0$ and $u = u_0$ (see the figure), chosen so that $\mathcal{S}$ intersects the initial vertex (v_0, u_0). The data are evolved using a finite-difference version of Eq. (25) that has a local discretization error of $O(h^4)$, leading to a quadratic convergence globally (i.e., the accumulated error scales like h^2). Our finite-difference scheme is precisely identical to the one used in Ref. [23] (as detailed in Appendix B therein) when applied to circular orbits. A detailed description of our scheme for generic orbits is provided in Appendix C (as applied to the modified version of the field equation that we end up solving in practice; see below). The appropriate jump conditions across $\mathcal{S}$ are implemented at the level of the finite-difference formula when it is applied to grid cells containing a segment of $\mathcal{S}$, as detailed in Appendix C 2. Our code takes as input the spin $s = \pm 2$; modal numbers ℓ, m; and orbital trajectory $R(t)$ (as well as a range of numerical parameters such as h and the coordinate ranges) and returns the Hertz potential modes $\phi^{+}_{\ell m}(t,r)$ (IRG) or $\phi^{-}_{\ell m}(t,r)$ (ORG).

The physical initial data for the evolution are not known in general, so we start with fictitious data on $v=v_0$ and $u=u_0$. Specifically, we set $\phi^{>}(v,u_0)\equiv 0$ and $\phi^{<}(v_0,u)\equiv 0$ and let the field be sourced by the imposed jumps along $\mathcal{S}$. This produces an outburst of "junk" radiation at the initial vertex (v_0,u_0). We expect such junk radiation to decay in time (with an inverse power law approximately $t^{-2\ell-3}$, theoretically [37]), leaving behind the desired physical solution at late time. The early, junk-contaminated part of the data is discarded.

Since our characteristic numerical domain has no timelike boundaries, there is no need to impose boundary conditions and no way to actively control violations away from the desired retarded solution. This is not a problem when all other ("nonphysical") vacuum solutions of the field equation decay at late time but can become a problem when there exist nonphysical solutions that fail to decay or, worse, grow at late time. Past implementations of 1 + 1D characteristic schemes for the scalar field equation (e.g., Ref. [38]), electromagnetic vector potential [39], Regge-Wheeler-Zerilli equations (e.g., Ref. [40]), and the Lorenz-gauge metric perturbation equations (e.g., [41]) show no signs of such troublesome modes. In these cases, the numerical solutions always appear to converge to the true, physical solution at late time.[4] As we demonstrate below, the situation with the $|s|=2$ Teukolsky equation is less fortunate: in our simple u, v-coordinate-based evolution, nonphysical modes of the equation, seeded by numerical error, will grow unbounded at late time, spoiling the evolution. We will discuss the origin of the problem and suggest ways around it.

Why was the problem not identified already in Ref. [23], which used the same numerical method? Our new code, when run with a circular-orbit source and $s=-2$, does reproduce the numerical results of Ref. [23] in the early stage of the evolution, before the onset of growth. We no longer have access to the code used in Ref. [23], but it appears that the evolutions performed in that study were simply too short to reveal the problem: the calculation of the Hertz potential along circular orbits did not require very long runs, and evolutions were always terminated before the relatively slowly growing mode (approximately t^4 for $s=-2$; see below) had a chance to manifest itself in the data. Calculations for scatter orbits require much longer evolutions, so here we must deal with the problem. The problem must be dealt with anyway if one is interested in an ORG reconstruction ($s=+2$), where, as discussed below, the blowup is exponential.

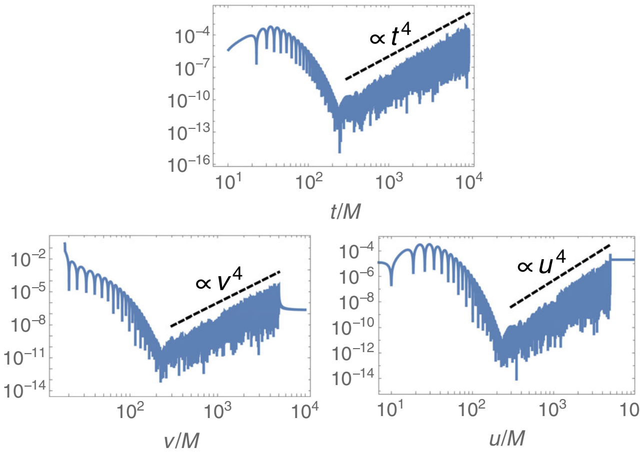

FIG. 2. Results from evolution of the $(\ell,m)=(2,0)$ mode of the vacuum 1 + 1D BPT equation with $s=-2$. The evolution is seeded with a narrow Gaussian near $(t,r_*)\sim(0,9M)$. We show, on a log-log scale, the field amplitude $|\phi^{-}_{20}|$ sampled along slices of constant $r_*=10M$ (top), $u=500M$ (lower left) and $v=500M$ (lower right). The dashed lines (const $\times\, t^4$, const $\times\, v^4$ and const $\times\, u^4$, respectively) are shown for reference.

In what follows, we illustrate the problem of growing modes with numerical examples and describe the range of tests we performed to understand its origin. We then discuss possible remedies. Since the issue arises already in vacuum evolutions—indeed, it is more easily seen in the absence of a particle source—we restrict the discussion in the rest of this chapter to the vacuum case.

B. Case $s=-2$ (vacuum)

Figure 2 shows a typical output from an $s=-2$ numerical evolution in vacuum, i.e., setting all jumps across $\mathcal{S}$ to zero. We seed the evolution with a narrow Gaussian pulse near the initial vertex at $(u_0,v_0)=(-9M,9M)$ [corresponding to $(t,r)\sim(0,7.12M)$] and evolve out to $(u,v)=(10^4M,10^4M)$. After the initial spike of radiation (not shown in the figures), the field decays with characteristic quasinormal ringing. However, at around $t\sim 250M$, the solution becomes dominated by a noisy component, whose amplitude appears to grow approximately like approximately t^4. The growth seems to continue indefinitely towards future timelike infinity ($t\to\infty$ with fixed $r>2M$), but the solution settles to a finite value approaching null infinity ($v\to\infty$ with fixed u) and also approaching the event horizon ($u\to\infty$ with fixed v). A similar behavior is observed for all values of ℓ and m and irrespectively of the choice of compact initial data. The evolution up to the onset of growth is numerically stable, and the solution there converges quadratically in grid spacing h, as expected. The growing component, however, is not numerically stable; it displays noisy features on grid-size scale, and its amplitude appears to

---

[4] Sole exceptions known to us are certain monopole and dipole gauge modes of the Lorenz-gauge metric perturbations, which grow linearly in time [21].

increase with decreasing h (finer resolution). The approximately t^4 behavior, however, seems to be persistent and universal.

We have performed a series of tests in attempt to understand these results. First, as mentioned, we have tried a variety of initial data, including a point seed at the initial vertex, smooth Gaussians of various configurations, and data corresponding to an exact static solution of the BPT equation. Second, we have tried a range of alternative finite-difference formulas and stepping schemes. Third, we have used our code to solve for the Weyl scalar modes $\psi^-(t,r)$ with jump conditions on $\mathcal{S}$ corresponding to a circular geodesic orbits (the necessary jump conditions are derived in Appendix B); we have done so both with "zero" initial data and with data corresponding to an exact static solution (for an $m=0$ mode). In all these tests, the t^4 growing mode developed just the same. Fourth, we note that the troublesome t^4 behavior is observed [42] also in the application to the Teukolsky equation of the recently introduced approach by O'Toole *et al.* [43], in which the Green's function (rather than the field itself) is evolved from exact characteristic initial data. Finally, we observe that we are, in fact, able to successfully suppress the t^4 growth (albeit at considerable computational cost) using our *Mathematica* implementation with very high working precision. All this supports the conclusions that (i) the t^4 behavior has a genuine dynamical origin and (ii) the t^4 component is seeded by numerical roundoff error.

We suggest that the t^4 mode represents nonphysical incoming radiation sourced by numerical roundoff error near $\mathcal{I}^+$. This can be seen from the following heuristics. First, recall from Eqs. (45) and (46) the asymptotic form of monochromatic $s=-2$ solutions in the "wave zone" ($r\gg M$ with $v\gg u$): $\phi\sim e^{-i\omega u}$ for physical solutions (purely outgoing waves) and $\phi\sim r^{-4}e^{-i\omega v}$ for nonphysical solutions representing purely incoming waves. More generally, the time-domain solutions are superpositions of such monochromatic modes and have the forms $\phi\sim F(u)$ (physical) and $\phi\sim r^{-4}G(v)$ (nonphysical) for some functions $F(u)$ and $G(v)$ that depend on the initial data. [These forms can be confirmed more directly by substituting the Ansätze $\phi=r^\alpha F(u)$ and $\phi=r^\beta G(v)$ into the BPT equation (25) and solving at leading order in M/r under the wave-zone assumptions $F'(u)\gg F(u)/r$ and $G'(v)\gg G(v)/r$, to obtain $\alpha=0$ and $\beta=-4$.] Consider an outgoing ray $u=\text{const}$ shortly after the start of the evolution. The field on this ray is composed mostly of outgoing radiation $\phi\sim F(u)$, which approaches a constant value at large v. However, the roundoff error in the numerical data along this ray will inevitably source a small component of nonphysical high-frequency incoming radiation $\phi\sim r^{-4}G(v)$. Since the sourcing field is asymptotically constant at $v\to\infty$, the amplitude of the seeded incoming radiation is also expected to be asymptotically constant on the $u=\text{const}$ ray, i.e., $r^{-4}|G(v)|\sim\text{const}$ for $v\to\infty$. This implies $|G(v)|\sim v^4\sim(t+r)^4$ at large v, and it follows that the incoming-wave component has an amplitude $|\phi|\sim v^4/r^4\sim(t+r)^4/r^4$. At fixed r, this will exhibit a $\sim t^4$ growth, at least in the wave zone where our heuristic analysis applies. (To show that this wave-zone behavior might lead to a t^4 growth elsewhere at late time, as evident in the numerical data, would require a more detailed asymptotic matching analysis, which we have not attempted.)

This heuristic description explains the results of our various experiments. The t^4 behavior arises dynamically from roundoff error seeds, so it is persistent, universal, and independent of initial data. The amplitude of the t^4 component can be suppressed by increasing the precision of the floating-point arithmetic, which reduces the roundoff error. For a fixed floating-point precision, increasing the grid resolution (decreasing h) enhances the amplitude of the incoming radiation component, by seeding more of its modes at higher frequencies.

It is also possible to explain why the t^4 growth does not appear to plague other time-domain treatments of the $s=-2$ Teukolsky equation reported in the literature. In the $2+1$-dimensional ($2+1$D) Cauchy evolution approach of Khanna *et al.* (legacy of Refs. [44,45] and many works since), boundary conditions are actively imposed, which presumably suppress the growth of the unphysical component. In the compactified hyperboloidal slicing approaches of Refs. [24–26], we suspect it is the *compactification* of $\mathcal{I}^+$ that averts the problem, since the wave zone for incoming waves is vastly under resolved on the compactified grid. In contrast, our simple u, v-coordinate-based approach resolves the wave zone equally well for both outgoing and incoming waves. Unfortunately, as we have seen, the resolution of incoming waves near null infinity is harmful in our case.

C. Case $s=+2$ (vacuum)

Figure 3 shows a typical output from an $s=+2$ numerical evolution in vacuum. Again, we start with a narrow Gaussian near the initial vertex at $(u_0,v_0)=(-9M,9M)$ and this time evolve out to $(u,v)=(10^3M,10^3M)$. In this case, after a short phase of quasinormal decay (harder to discern on the semilogarthmic scale of Fig. 3), there commences a rapid exponential growth, $\phi\sim\exp[t/(2M)]$. Again, the growth seems to continue indefinitely toward future timelike infinity ($t\to\infty$ with fixed $r>2M$), but the solution settles to finite values toward $\mathcal{I}^+$ and $\mathcal{H}^+$. A similar behavior is observed for all values of ℓ and m and all choices of initial data we have tried, and the blowup exponent $(1/2M)$ seems universal. The growing component is not numerically stable, increasing in amplitude with decreasing h (finer resolution). We have performed similar tests to the ones described above for $s=-2$ and with similar results: The exponential growth is persistent and universal

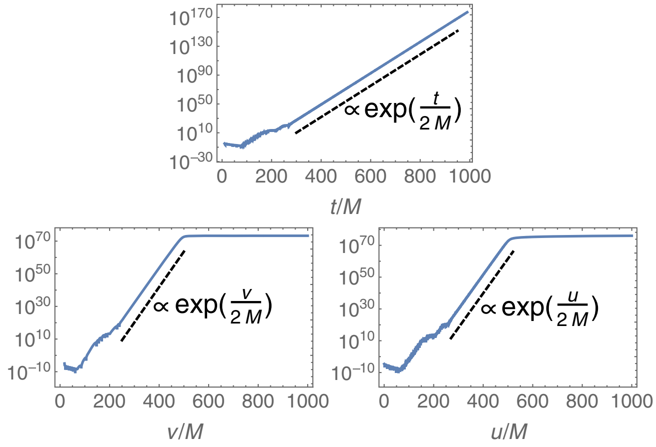

FIG. 3. Results for the evolution of the $(\ell, m) = (2, 0)$ mode of the vacuum $1 + 1$D BPT equation with $s = +2$. Other details are as in Fig. 2, except here the scale is semilogarithmic. The dashed lines are for reference.

and can be moderated (in amplitude) only with high-precision arithmetic.

We again argue that the culprit is a nonphysical growing solution of the BPT equation seeded by roundoff error, this time an exponential mode of the $s = +2$ equation. We can see this most instructively from a simple asymptotic analysis near the horizon, as follows. Working at leading order in Δ and assuming ϕ, $\phi_{,u}$, and $\phi_{,v}$ are all of the same order in Δ near the horizon [this is true of the $r \to 2M$ asymptotic expressions in Eq. (45) and (46)], the BPT equation (25) reduces to

$$\phi_{,uv} - k\phi_{,u} = 0, \tag{73}$$

in which $k \coloneqq s/(4M)$ and where we have retained the s dependence to enable us to compare the situation between the two spin values. The general solution is

$$\phi = C_1(u)e^{kv} + C_2(v), \tag{74}$$

where $C_1(u)$ and $C_2(v)$ are arbitrary functions. Solutions of the form $\phi = C_2(v)$ represent physical perturbations that are purely ingoing at the horizon [compare with Eq. (45)], while solutions of the form $\phi = C_1(u)e^{kv}$ represent nonphysical perturbations coming out of the past horizon [compare with Eq. (46), noting $\Delta^s \sim (2M)^{2s}e^{2kr_*} \sim (2M)^{2s}e^{kv}$ near the horizon]. For $s = +2$, the nonphysical solution blows up exponentially in v along the horizon, while for $s = -2$, it is exponentially suppressed.

The situation now mirrors what we had near null infinity for the $s = -2$ growth: as the main physical perturbation, of the form $\phi = C_2(v)$, reaches the horizon, roundoff error along the incoming ray seeds a nonphysical component $\sim C_1(u)e^{kv}$, which, for $s = +2$, blows up exponentially along the horizon. The predicted rate of exponential growth is consistent with that observed in the numerical data: approximately $e^{sv/(4M)} = e^{v/(2M)}$. To understand the propagation of this exponential growth into other areas of the black hole's exterior would require a detailed asymptotic matching analysis, but it would not be surprising to find a similar exponential growth in time anywhere outside the black hole, as seen in the numerics. We note the fortunate situation in the $s = -2$ case, where all nonphysical modes are exponentially suppressed in a dynamical manner, with no need to actively impose boundary conditions.

There are in the literature several successful time-domain numerical methods for the $s = +2$ Teukolsky equation (e.g., Refs. [26,46–48]), all incorporating horizon-penetrating coordinates in some form. The use of such coordinates (effectively a compactification of our u, v coordinates) under-resolves any outgoing component of the perturbation field near the horizon, thereby avoiding the problem encountered here.

D. Mitigation

Although initially surprising to us, it is clear that a standard unigrid characteristic evolution based on u, v coordinates does not work well for either $s = +2$ or $s = -2$ Teukolsky equations. A remedy based on the use of very high-precision arithmetic is clearly impracticable. The preceding discussion and evidence from the literature suggest that compactification of the two asymptotic domains ($\mathcal{I}^+$ and $\mathcal{H}^+$) can offer a solution that is both computationally efficient and practicable. This has already been achieved, e.g., by Harms *et al.* [26], using asymptotically null compactified spacelike slices. It is perceivable that the same could also be achieved within the convenient framework of a fully double-null architecture. This approach is worth exploring.

Here, we choose to apply a different strategy. Instead of tackling the BPT equation directly, we will introduce a transformation of the Hertz potential to a new field variable, which satisfies a field equation free of the above difficulties. From the preceding discussion, it is clear that the culprit term in the BPT equation (in both $s = -2$ and $s = +2$ cases) is the one involving $\phi_{,t}$, so we seek a transformation that eliminates that term. The simplest such transformation is a time-domain version of the familiar Chandrasekhar transformation [49], which takes solutions of the BPT equation to solutions of the Regge-Wheeler (RW) equation. As we have mentioned, the RW equation evolves without a problem on a simple uniform mesh based on u, v coordinates (see, e.g., Ref. [40]), so this approach would require no radical architectural changes to our numerical method.

In the next section, we reformulate the $1 + 1$D no-string evolution problem in terms of a RW-like variable. Then, in Sec. VII, we demonstrate a full numerical calculation of the Hertz potential for a scatter orbit.

VI. REFORMULATION IN TERMS OF A RW-LIKE VARIABLE

Let the field $X(t,r)$ be a solution of the vacuum Regge-Wheeler equation

$$X_{,uv} + \frac{f}{4}\left(\frac{\lambda_1}{r^2} - \frac{6M}{r^3}\right)X = 0, \tag{75}$$

where, recall, $f = 1–2M/r$ and $\lambda_1 = \ell(\ell+1)$. Then, as can be easily checked,

$$\phi_+ = \frac{1}{4r}\tilde{\boldsymbol{D}}_n^2(rX) = f^{-2}\left(X_{,uu} - \frac{r-3M}{r^2}X_{,u}\right) \tag{76}$$

and

$$\phi_- = \frac{f^2 r^3}{4}\boldsymbol{D}_\ell^2(rX) = r^4\left(X_{,vv} + \frac{r-3M}{r^2}X_{,v}\right) \tag{77}$$

are solutions of the vacuum BPT equation (25) with $s = -2$ and $s = +2$, respectively. This means that we can use the RW variable X as a generating function for both the IRG Hertz potential ϕ_+ and ORG Hertz potential ϕ_- in each of the vacuum regions $\mathcal{S}^{\gtrless}$. The advantage, of course, is that the RW equation (75), unlike the BPT equation (25), does lend itself to a straightforward characteristic evolution in u, v coordinates. The idea now would be to formulate a suitable characteristic initial-value problem for the RW variable X, from which the no-string Hertz potential $\phi_+^{\gtrless}$ (or $\phi_-^{\gtrless}$) can be obtained by applying the transformation (76) [or (77)] to vacuum RW solutions $X^{\gtrless}$ in the corresponding vacuum domains $\mathcal{S}^{\gtrless}$. To achieve this, X must satisfy appropriate jump conditions along $\mathcal{S}$ and suitable boundary conditions at $\mathcal{I}^+$ and $\mathcal{H}^+$.

A. Boundary conditions

Let us consider boundary conditions first. In both asymptotic regions $r \to \infty$ and $r \to 2M$, monochromatic solutions of the RW equation (75) are superposition of modes $X \sim e^{-i\omega u}$ and $X \sim e^{-i\omega v}$ (with some generally nonzero constant coefficients at leading order). The "retarded" monochromatic solution has the behavior $X \sim e^{-i\omega u}$ near $\mathcal{I}^+$ and $e^{-i\omega v}$ near $\mathcal{H}^+$. It it easily seen that this retarded solution generates the physical IRG Hertz potential $\phi_+ \sim e^{-i\omega u}$ near $\mathcal{I}^+$ and the physical ORG Hertz potential $\phi_- \sim e^{-i\omega v}$ near $\mathcal{H}^+$ [here, we recall Eq. (45)]. It is harder to show that the retarded RW solution necessarily generates the physical field ϕ_+ near $\mathcal{H}^+$ or the physical field ϕ_- near $\mathcal{I}^+$ (this would require a higher-order asymptotic analysis), but we can circumvent this with the following observation: from Eq. (46), we see that nonphysical modes of the IRG potential ϕ_+ diverge (like Δ^{-2}) near $\mathcal{H}^+$ and that the nonphysical modes of the ORG potential ϕ_- diverge (like r^4) near $\mathcal{I}^+$. Thus, in either case, a nonphysical Hertz potential announces its presence loudly in the form of a strong asymptotic divergence. This is a point made already in Ref. [23]: a solution ϕ_+ that is regular (bounded) at $\mathcal{H}^+$ is automatically the physical one, and so is a solution ϕ_- that is regular (bounded) at $\mathcal{I}^+$. We can establish *a posteriori* that our numerical solutions $\phi_+^<$ or $\phi_-^>$ satisfy physical boundary conditions simply by checking they are bounded.

In summary, we propose that the required vacuum RW solutions on $\mathcal{S}^>$ and $\mathcal{S}^<$ are the ones satisfying standard, retarded boundary conditions at $\mathcal{I}^+$ and $\mathcal{H}^+$, respectively. For the IRG potential ϕ_+, this is guaranteed on $\mathcal{S}^>$ and can be easily checked *a posteriori* on $\mathcal{S}^<$. For the IRG potential ϕ_-, this is guaranteed on $\mathcal{S}^<$ and can be easily checked *a posteriori* on $\mathcal{S}^>$.

B. Jumps across $\mathcal{S}$

It remains to translate the jumps in ϕ and its derivatives across $\mathcal{S}$, obtained in Sec. IV, to jumps in X and its derivatives there. For brevity, we only discuss here the IRG case, but jumps for the ORG case can be obtained in a similar manner.

We could not find an explicit inverse of the transformation (76), but (given ϕ_+) it is easy to obtain two independent algebraic relations between X, $X_{,u}$, and $X_{,v}$, which will suffice for our purpose. First, taking ∂_v of (76) and using (75) and (76) to substitute for $X_{,uv}$ and $X_{,uu}$, respectively, leads to

$$X_{,u} = \frac{f}{r(\lambda r + 6M)}(3MX - 8Mr^2\phi_+ - 4r^4\phi_{+,v}), \tag{78}$$

where, recall, $\lambda = (\ell+2)(\ell-1)$. Second, taking ∂_{vv} of (76), then using the u and v derivatives of the RW equation (75) to replace for $X_{,uvu}$ and $X_{,uvv}$, and finally using (75) and (76) again to replace for $X_{,uv}$ and $X_{,uu}$, we obtain

$$\begin{aligned} X_{,v} = -\left(\alpha + \frac{3Mf}{r(\lambda r + 6M)}\right)X + \frac{8Mr(\lambda+3)}{3(\lambda r + 6M)}\phi_+ \\ + \frac{4r^3[\lambda r + (\lambda+9)M]}{3M(\lambda r + 6M)}\phi_{+,v} + \frac{4r^4}{3M}\phi_{+,vv}. \end{aligned} \tag{79}$$

By applying Eqs. (78) and (79) in both vacuum sides of $\mathcal{S}$ in the limit to $\mathcal{S}$, we obtain relations between the jumps $[X_{,u}]$ and $[X_{,v}]$ on the one hand and the jumps $[X]$, $[\phi_+]$, $[\phi_{+,v}]$ and $[\phi_{+,vv}]$ (the latter three assumed known) on the other hand; these relations are obtained by simply replacing $X \mapsto [X]$, etc., in Eqs. (78) and (79), and setting $r \mapsto R(t)$ there.

Now, along the orbit, we also have the relation

$$[\dot{X}] = [X_{,t}] + \dot{R}_*[X_{,r_*}], \tag{80}$$

where, recall, an overdot denotes d/dt. Using $[X_{,t}] = [X_{,v}] + [X_{,u}]$ and $[X_{,r_*}] = [X_{,v}] - [X_{,u}]$ and substituting $[X_{,u}]$ and $[X_{,v}]$ from Eqs. (78) and (79), we thus obtain a simple first-order ODE for the jump $[X]$ along the orbit, of the form [compare with (60)]

$$\dot{[X]} + (A_X(R)\dot{R}_* + \alpha)[X] = \mathcal{F}_X. \tag{81}$$

The coefficient A_X here is given by

$$A_X = \alpha + \frac{6M(R-2M)}{R^2(\lambda R + 6M)}, \tag{82}$$

and the sourcing function $\mathcal{F}_X$ involves the known jumps in the Hertz potential and its derivatives,

$$\begin{aligned}\mathcal{F}_X = {} & \frac{8M[6M(f_R - \dot{R}) + R(\lambda(f_R + \dot{R}) + 6\dot{R})]}{3f_R(\lambda R + 6M)}[\phi_+] \\ & + \frac{4R^2}{3Mf_R(\lambda R + 6M)}[6M^2(f_R - \dot{R}) \\ & + \lambda R(M+R)(f_R + \dot{R}) + 6MR(f_R + 2\dot{R})][\phi_{+,v}] \\ & + \frac{4R^4(f_R + \dot{R})}{3Mf_R}[\phi_{+,vv}],\end{aligned} \tag{83}$$

where $f_R \coloneqq f(R) = 1\text{–}2M/R$.

Equation (81) admits simple homogeneous solutions, given by (any constant multiple of)

$$[X]_h = \left(\lambda + \frac{6M}{R}\right)e^{-\alpha(t+R_*)}. \tag{84}$$

Note that all these homogeneous solutions (except the trivial zero one) blow up exponentially at $t \to -\infty$. There is a unique particular solution of the full inhomogeneous equation (81) that remains bounded; it is given by

$$[X] = [X]_h \int_{-\infty}^{t} \frac{\mathcal{F}_X(t')}{[X]_h} dt'. \tag{85}$$

This describes the jump in the RW variable needed for it to reproduce the no-string Hertz potential.

In practice, we find it easier to calculate $[X]$ not from Eq. (85) but via a numerical integration of the first-order ODE (81). It is best to integrate forward in time from $t \to -\infty$, going against the direction of exponential growth of the homogeneous solutions (84), in order to prevent the growth of such nonphysical modes from numerical error. For this integration, we need an initial condition at $t \to -\infty$, which in the case of a scatter orbit corresponds to $R \to \infty$ (with $\dot{R}_\infty < 0$). The condition is obtained from a simple asymptotic analysis of the ODE (81): assuming $[X]$ has a power-law behavior at infinity, we have $\dot{[X]} \ll [X]$ at large R, so the derivative term in (81) may be dropped at leading order. Then, using the $R \to \infty$ limits $A_X \to \alpha$ and

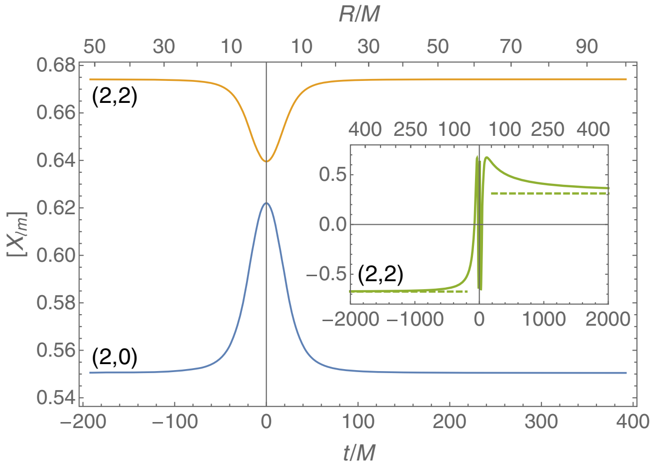

FIG. 4. The modulus of the jump $[X_{\ell m}]$ in the no-string field $X_{\ell m}$ along the geodesic scatter orbit depicted in Fig. 5, for the $(\ell, m) = (2, 0)$ and (2,2) modes. This is obtained by numerically integrating the first-order ODE (81) forward in time with the initial condition (87) at large negative t and $\varphi_{\text{in}} = 0$. As a check, the solution approaches the asymptotic value given in (87) with $\varphi_{\text{out}} \simeq 481°$ (obtained by integrating the geodesic equation). The inset plot demonstrates this for the real part of $[X_{22}]$, with dashed lines indicating the analytical asymptotic values. This jump function inputs into our 1 + 1D characteristic evolution scheme, whose application is illustrated in Sec. VII.

$$\mathcal{F}_X \to -\frac{16\pi\mu E}{3M\sqrt{\lambda_2}}(1 + \dot{R}_\infty)\bar{Y} \tag{86}$$

[obtained with the help of Eqs. (70)–(72)], we arrive at

$$[X]_{R\to\infty} = -\frac{64\pi\mu E}{\lambda_2^{3/2}}\bar{Y}_{\ell m}\left(\frac{\pi}{2}, \varphi_{\text{in/out}}\right), \tag{87}$$

which applies with φ_{in} for $t \to -\infty$ and with φ_{out} for $t \to +\infty$. In our implementation, we use (87) to set the initial value of $[X]$ at $t \to -\infty$,[5] integrate the ODE (81) forward in time, and then use (87) again to check the result of integration at $t \to +\infty$. Figure 4 illustrates the result of applying this procedure along a particular strong-field scatter orbit (the one depicted in Fig. 5 further below).

Once we have $[X]$, it is straightforward to get jumps in derivatives of the field, also needed for our 1 + 1D evolution scheme. This can be done algebraically. From Eqs. (78) and (79), one immediately gets $[X_{,u}]$ and $[X_{,v}]$, and using the RW equation (75), one gets $[X_{,uv}]$. The jump $[X_{,uu}]$ is subsequently obtained from the transformation

---

[5] In practice, we impose our boundary condition at a sufficiently large negative value of t with φ_{in} calculated at the start point by integrating the geodesic equation (89) from $t = -\infty$.

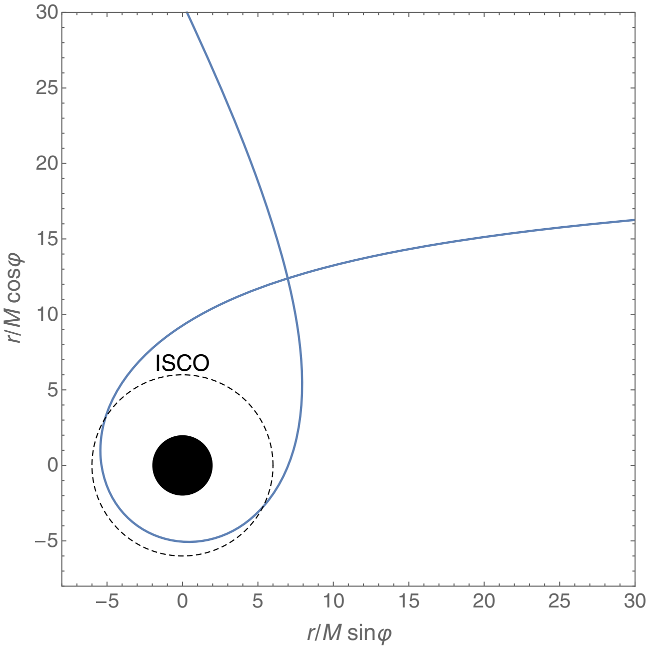

FIG. 5. The sample scatter geodesic orbit used for our numerical illustration, with parameters given in Eqs. (102) and (103). The orbit is plotted in the equatorial plane using Cartesian-like coordinates $(x, y) = (r\cos\varphi, r\sin\varphi)$. The location of the innermost stable circular orbit (ISCO) is shown for reference. The deflection angle of this strong-field orbit is $\delta\varphi \simeq 301°$.

equation (76), and $[X_{,vv}]$ can be found from the v derivative of Eq. (79). The jumps in the third and higher derivative can be found recursively in a similar manner.

VII. NUMERICAL IMPLEMENTATION FOR SCATTER ORBITS

We now present a full implementation of our method for a strong-field geodesic scatter orbit. Our code takes as input the parameters of the geodesic orbit, along with multipolar numbers ℓ, m, and returns the generating-function fields $X^{\gtrless}_{\ell m}(t, r)$ and the IRG no-string modal Hertz-potential fields $\psi^{\gtrless}_{\ell m}(t, r)$. In what follows, we first review hyperbolic geodesic orbits in Schwarzschild spacetime, then describe the details of our numerical algorithm, and finally present a sample of numerical results.

A. Hyperbolic-type geodesic orbits

In Schwarzschild spacetime, we consider a timelike geodesic orbit that starts and ends at infinity. We set our Schwarzschild coordinates so that the orbit lies in the equatorial plane, $\theta = \pi/2$. The orbit is then described by the two functions $r = R(t)$ and $\varphi = \varphi_p(t)$, which satisfy

$$\dot{R} = \pm\frac{f_R}{E}\sqrt{E^2 - \frac{f_R(R^2 + L^2)}{R^2}}, \tag{88}$$

$$\dot{\varphi}_p = \frac{f_R L}{R^2 E}, \tag{89}$$

where (recall) an overdot denotes d/dt. Here, we have parametrized the geodesic orbit with the two constants of motion E and L, respectively, the specific energy and angular momentum. For a scatter orbit $E > 1$, and without loss of generality, we have taken $L > 0$, and, correspondingly, $\dot{\varphi}_p > 0$. The sign in (88) switches from $-$ to $+$ at the periastron, where $\dot{R} = 0$. The particle scatters back to infinity (and does not fall into the black hole) if and only if $L > L_{\rm crit}(E)$, where

$$L_{\rm crit} = M\left(\frac{27E^4 + 9\zeta E^3 - 36E^2 - 8\zeta E + 8}{2(E^2 - 1)}\right)^{1/2}, \tag{90}$$

with $\zeta \coloneqq \sqrt{9E^2 - 8}$. The function $L_{\rm crit}(E)$ is monotonically increasing, so the minimum possible value of L is $L_{\rm crit}(E \to 1) = 4M$.

An alternative, more physically intuitive parametrization is provided by the initial incoming speed at infinity,

$$v_\infty \coloneqq |\dot{R}(t \to -\infty)| = \frac{\sqrt{E^2 - 1}}{E}, \tag{91}$$

and impact parameter,

$$b \coloneqq \lim_{t\to-\infty} R(t)\sin|\varphi_p(t) - \varphi_{\rm in}| = \frac{L}{\sqrt{E^2 - 1}}, \tag{92}$$

where $\varphi_{\rm in} \coloneqq \varphi_p(t \to -\infty)$. Note $E = (1 - v_\infty^2)^{-1/2}$, so E is the usual gamma factor at infinity. For a scatter orbit, we need $b > b_{\rm crit} = L_{\rm crit}(E)/\sqrt{E^2 - 1}$. The function $b_{\rm crit}(E)$ is monotonically decreasing, so the minimal possible value of b is $b_{\rm crit}(E \to \infty) = 3\sqrt{3}M \simeq 5.196M$.

For a scatter orbit, the equation $\dot{R} = 0$ admits a single real root outside the horizon, corresponding to the periastron radius $R = R_{\rm min}$. Given E and L, this radius can be expressed in the convenient form [50]

$$R_{\rm min} = \frac{6M}{1 - 2\sqrt{1 - 12M^2/L^2}\,\sin\left(\frac{\pi}{6} - \frac{1}{3}\arccos\beta\right)}, \tag{93}$$

where

$$\beta = \frac{1 + (36 - 54E^2)M^2/L^2}{(1 - 12M^2/L^2)^{3/2}}. \tag{94}$$

It can be checked that, for any fixed $E > 1$, β is a monotonically increasing function of L, varying between $\beta = -1$ for $L = L_{\rm crit}(E)$ and $\beta = +1$ for $L \to \infty$; hence, the expression in (93) is manifestly real, and $R_{\rm min}$ increases monotonically with L at fixed E and decreases monotonically with E at fixed L. The smallest periastron distance achievable is $R_{\rm min} \to 3M$, for $L \to L_{\rm crit}(E)$ with $E \to \infty$. Without loss of generality, we set $t = 0$ at the periastron passage, i.e., take $R(0) = R_{\rm min}$.

Another convenient parametrization of scatter orbits employs the eccentricity, $e > 1$, and (a-dimensionalized) semilatus rectum, $p > 6 + 2e$, defined from

$$R_{\rm min} = \frac{Mp}{1+e}, \qquad R_- = \frac{Mp}{1-e}, \tag{95}$$

where R_- is the negative root of $\dot{R} = 0$. [For a scatter orbit, i.e., one with $E > 1$ and $L > L_c(E)$, $\dot{R} = 0$ admits three real roots: $R_{\rm min}$, R_-, and (say) R_3 (in addition to the trivial root at $R = 2M$), satisfying $R_- < 0 < R_3 < 2M < R_{\rm min}$.] The relations with E and L are

$$E^2 = \frac{(p-2)^2 - 4e^2}{p(p-3-e^2)}, \qquad L^2 = \frac{p^2M^2}{p-3-e^2}. \tag{96}$$

In terms of e and p, the radial motion takes the convenient Keplerian-like form

$$R(t) = \frac{Mp}{1 + e\cos\chi(t)}. \tag{97}$$

The "anomaly" parameter χ increases monotonically in t along the orbit, running over $\chi \in (-\chi_\infty, \chi_\infty)$ for $t \in (-\infty, \infty)$, with $\chi_\infty = \arccos(-1/e)$ and $\chi = 0$ at the periastron passage. The relations $t(\chi)$ and $\varphi_p(\chi)$ can be determined by integrating

$$\frac{dt}{d\chi} = \frac{Mp^2}{(p-2-2e\cos\chi)(1+e\cos\chi)^2}\sqrt{\frac{(p-2)^2 - 4e^2}{p-6-2e\cos\chi}}, \tag{98}$$

$$\frac{d\varphi_p}{d\chi} = \sqrt{\frac{p}{p-6-2e\cos\chi}}, \tag{99}$$

with the initial conditions $t(-\chi_\infty) = -\infty$ [or $t(0) = 0$] and $\varphi_p(-\chi_\infty) = \varphi_{\rm in}$. Finally, defining the scatter (or deflection) angle by $\delta\varphi := \varphi_{\rm out} - \varphi_{\rm in} - \pi$, one obtains, using Eq. (99),

$$\delta\varphi = \int_{-\chi_\infty}^{\chi_\infty} \frac{d\varphi_p}{d\chi} d\chi - \pi = 2k\sqrt{p/e}\,\mathsf{El}_1\left(\frac{\chi_\infty}{2}; -k^2\right) - \pi, \tag{100}$$

where $k := 2\sqrt{e/(p-6-2e)}$ and El_1 is the incomplete elliptic integrals of the first kind,

$$\mathsf{El}_1(\varphi; k) = \int_0^\varphi (1 - k\sin^2 x)^{-1/2} dx. \tag{101}$$

For the numerical demonstration to be presented below, we have picked a sample strong-field scatter geodesic with

$$v_\infty = 0.2 \quad \text{and} \quad b = 21M, \tag{102}$$

corresponding to

$$R_{\rm min} \simeq 4.9228M, \qquad E \simeq 1.02062, \qquad L \simeq 4.28661M,$$
$$e \simeq 1.1948, \qquad p \simeq 10.9351 \quad \text{and} \quad \delta\varphi \simeq 301°. \tag{103}$$

The orbit is depicted in Fig. 5.

B. Numerical algorithm

Our method is based on a characteristic numerical evolution in u, v coordinates, as described in Sec. V A—only here we are evolving the RW equation (75) instead of the BPT equation, and we impose suitable jump conditions along $\mathcal{S}$ (see Fig. 1) compatible with the no-string IRG solution for our sample scatter orbit. A detailed description of our finite-difference scheme is given in Appendix C, where we also explain how the jump conditions are incorporated into the scheme so as to achieve a (global) quadratic rate of numerical convergence. Here, we lay out the main steps of the numerical algorithm:

Input. The code takes as input the two orbital parameters v_∞ and b; the orbital radius $r = R_{\rm init}$ at the start (and end) of the numerical evolution; the field's multiple numbers ℓ, m; and the finite-difference interval $h := \Delta u = \Delta v$.

Step 1: Calculate geodesic orbit. Given v_∞ and b, the code calculates E and L and from these e and p, as well as $R_{\rm min}$. The functions $R(t)$ and $\varphi_p(t)$ are then derived in the range $R_{\rm min} \le R \le R_{\rm init}$ by numerically integrating $\dot{R}$ and $\dot{\varphi}_p$ as obtained from Eqs. (97)–(99), with initial conditions $R(0) = R_{\rm min}$ and $\varphi_p(-\infty) = 0$. The code also calculates $t_{\rm tot}$, the time it takes the particle to get from $R_{\rm init}$ back to $R_{\rm init}$ after being scattered.

Step 2: Set characteristic grid. The code then prepares a 2×2 array of u, v coordinate values representing the nodes of the characteristic mesh shown in Fig. 1. For the initial rays, we take $v_0 = -t_{\rm tot}/2 + R^*_{\rm init}$ and $u_0 = -t_{\rm tot}/2 - R^*_{\rm init}$ with $R^*_{\rm init} := r_*(R_{\rm init})$. This is so that the initial vertex $(u, v) = (u_0, v_0)$ is crossed by the particle at $(t, r) = (-t_{\rm tot}/2, R_{\rm init})$. The stepping interval is set at h, and the grid's dimensions are taken such that the final characteristic rays are at $u = t_{\rm tot}/2 - R^*_{\rm init}$ and $v = t_{\rm tot}/2 + R^*_{\rm init}$—so that the particle crosses the upper vertex at $(t, r) = (t_{\rm tot}/2, R_{\rm init})$ on its way out. Finally, the coordinate values of all intersections of the orbit with grid lines are calculated and stored.

Step 3: Obtain $[\phi]$ along the orbit. Using the analytical expressions in Appendix B, we calculate the jumps in the Weyl scalars $\psi_\pm$ and their derivatives along the orbit, for the ℓ, m mode in question. Specifically, we compute $[\psi_-]$

and $[\partial_u^n \psi_+]$ for $n = 0, \ldots, 3$, and from these, using (61), we analytically construct the source function $\mathcal{F}(t)$ in Eq. (60). We next numerically integrate the first-order ODE (60) with the initial condition (70), to obtain the jump $[\phi_+]$ in the Hertz potential along the orbit. From $[\phi_+]$, we algebraically obtain also $[\phi_{+,v}]$ and $[\phi_{+,vv}]$ using the procedure described in the last paragraph of Sec. IV. B.

Step 4: Obtain $[X]$ *along the orbit.* We now construct the source function $\mathcal{F}_X$ using Eq. (83) and then numerically solve the first-order ODE (81) for $[X]$ with the initial condition (87). From $[X]$, we algebraically obtain also $[X_{,v}]$, $[X_{,u}]$, $[X_{,vv}]$, $[X_{,uv}]$, and $[X_{,uu}]$, using the procedure described in the last paragraph of Sec. VI. B. The jump values are computed at all intersections of the particle's worldline with grid lines and stored as vector datasets.

Step 4: Obtain the generating function $X^{\gtrless}_{\ell m}$. We evolve the RW equation (75) using the second-order-convergent finite-difference scheme described in Appendix C. The scheme requires as input the field jumps calculated in the previous step at intersections of the worldline with grid lines. The evolution starts with zero initial data along $v = v_0$ and $u = u_0$ and proceeds along successive lines of $u = \text{const}$. The outcome is a finite-difference approximation to the generating field X in each of the vacuum regions $\mathcal{S}^>$ and $\mathcal{S}^<$.

Step 5: Derive the Hertz potential $\phi^{\gtrless}_{\ell m}$. Given X, the Hertz potential mode ϕ is calculated in each of the two vacuum regions using Eq. (76), where derivatives are taken numerically.

Output. In principle, the code can make available the Hertz potential ϕ anywhere in the computational domain. For our initial tests and for the purpose of illustration in this paper, we output both X and ϕ as functions of t along the orbit (on either of its sides) and as functions of u along the final $v = \text{const}$ ray (approximating $\mathcal{J}^+$).

C. Sample results

All of the results displayed here are for the orbit shown in Fig. 5, with parameters given in Eqs. (102) and (103). In all of the figures shown below, we have set $\mu = 1$ and $M = 1$ for convenience; as a result, in particular, t, R, and h are expressed in units of M.

Figure 6 demonstrates the behavior of the field $X^>_{\ell m}$ along the worldline of the particle, for a sample of ℓ, m values (the field $X^<_{\ell m}$ has a similar behavior). The evolution begins when the incoming particle is at $R_{\text{init}} = 100M$ and ends when the outflying particle is back at $100M$.

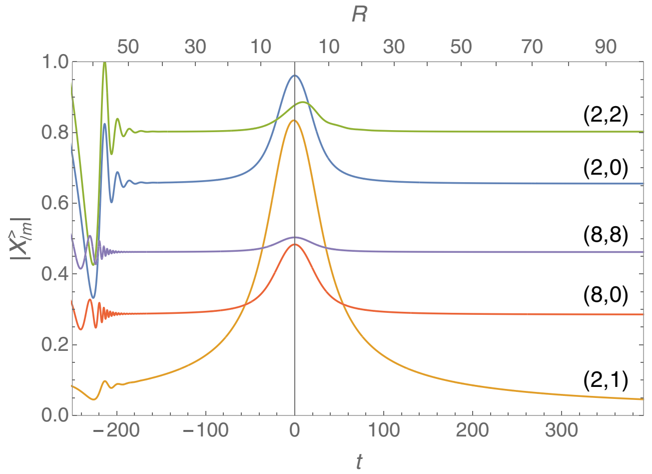

FIG. 6. The RW field $X_{\ell m}$ along the particle's worldline for the orbit shown in Fig. 5 and a sample of (ℓ, m) values. Here, we show $|X^>_{\ell m}(t, R(t))|$ as a function of time t (lower scale) and orbital radius R (upper scale). Curves are labeled with their (ℓ, m) values, with $\ell = 8$ data shown amplified by a factor ×600. The periastron location at $t = 0$ is indicated with a vertical line. The early part of the data is contaminated by initial junk radiation, and it is to be discarded.

We have performed convergence tests to confirm that our code exhibits a quadratic global convergence rate in h, as it is designed to do. An example is shown in Fig. 7. The global rate of convergence is very sensitive to the implementation details of the jump conditions in the finite-difference scheme (see Appendix C), so the observed quadratic convergence provides important reassurance that these jumps are implemented correctly.

As can be seen in Fig. 6, initially the data are contaminated by spurious waves, which, however, decay over time to reveal the true, physical solution. The decay appears faster for higher values of ℓ, as expected from theory. Figure 8 illustrates how, reassuringly, the "clean" part of the data appears to be insensitive to the value of R_{init}, up to a

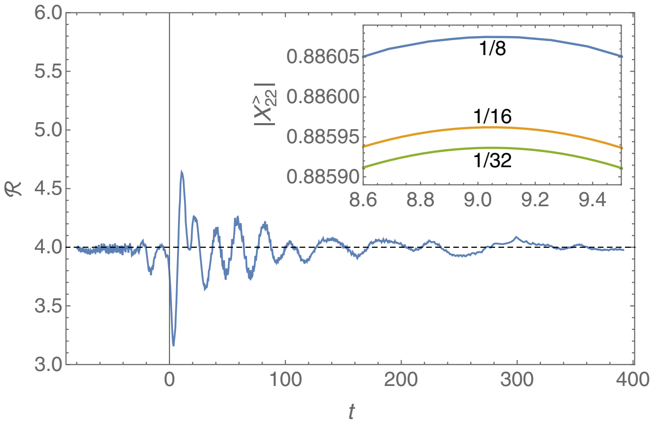

FIG. 7. Convergence test for the $(\ell, m) = (2, 2)$ numerical solution. The inset shows a detail from the $|X^>_{22}|$ (green) curve in Fig. 6, for a sequence of runs with decreasing grid spacing, $h = \{\frac{1}{8}, \frac{1}{16}, \frac{1}{32}\}M$. The main plot quantifies the convergence rate; it shows the ratio $\mathcal{R} := |X^>_8 - X^>_{16}|/|X^>_{16} - X^>_{32}|$ as a function of t along the orbit, where a subscript 8 (for example) denotes a calculation with grid spacing $h = M/8$. A ratio of $\mathcal{R} = 4$ is indicative of quadratic convergence.

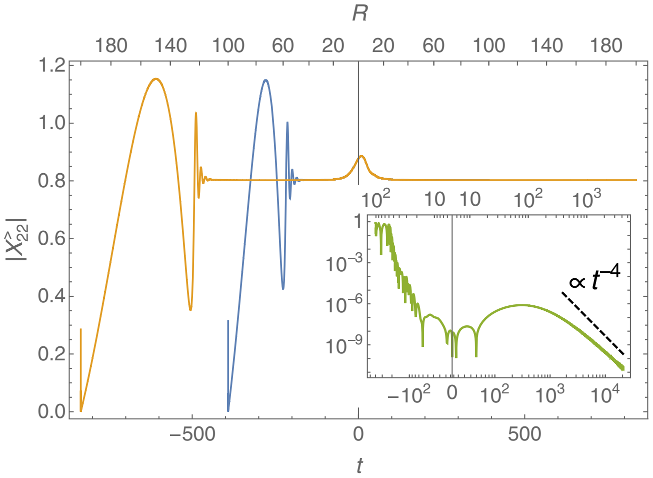

FIG. 8. Numerical results for $|X^{>}_{22}|$ on the particle's worldline, as calculated with $R_{\rm init} = 100M$ (blue) and with $R_{\rm init} = 200M$ (orange). The comparison illustrates how, reassuringly, the clean portion of the data is insensitive to $R_{\rm init}$, up to a small error that dies off in time. The inset displays the relative difference between the two curves, showing a t^{-4} falloff at late time, consistent with the theoretically predicted $t^{-\ell-2}$ decay rate for compact vacuum perturbation along a curve $r = R \propto t$ (see, for instance, Eq. (89) of Ref. [51]).

small decaying difference. As the figure demonstrates, using $R_{\rm init}$ as a control parameter enables us in practice to evaluate the level of residual contamination from initial junk.

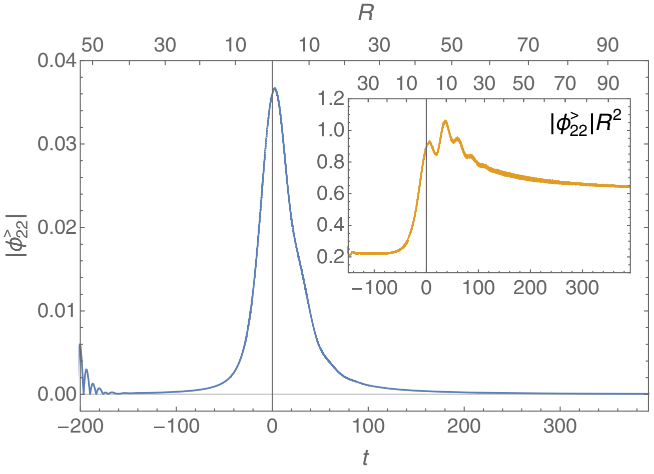

FIG. 9. The modulus of the no-string IRG Hertz potential $\phi^{>}_{22}$ along the particle's worldline. The field falls off as $X \sim t^{-2}$ at large R. The inset shows the same data rescaled by a factor $(R/M)^2$. The field exhibits the lagging peak and postperiastron undulation features discussed in the text. (The multiplication by R^2 makes more distinct the undulation feature, only barely visible in the main plot.)

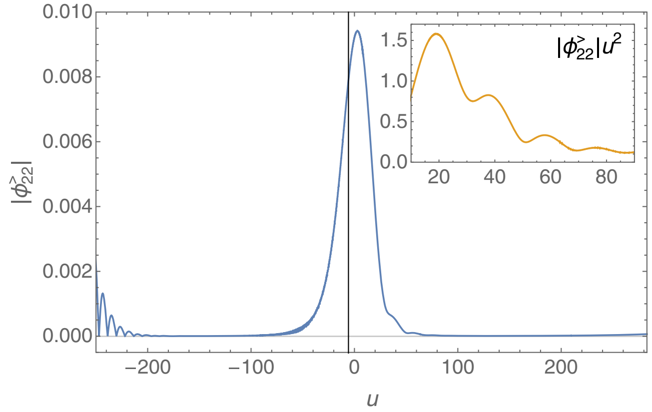

FIG. 10. The modulus of the Hertz potential $\phi^{>}_{22}$ as a function of u at $v = \text{const} = 499M$ (approximating $\mathcal{I}^+$). The vertical line represents u at periastron. The inset shows the same data rescaled by a factor $(u/M)^2$ to again highlight the postperiastron undulation feature.

Figure 9 shows the no-string IRG Hertz potential $\phi^{>}_{22}$ derived from $X^{>}_{22}$, as a function along the orbit. Notable physical features include (i) the small lag between the peak of the field and the periastron passage and (ii) the small undulation in the field amplitude not long after periastron passage. (Both features are visible already at the level of the generating function X and are numerically stable.) The periastron lag has been observed before in calculations along eccentric orbits (see, e.g., Ref. [41]); it is attributed to the effect of "tail" contributions to the self-field, which peak in amplitude soon after periastron. The undulation, we suggest, is a weak manifestation of the quasinormal-mode excitation phenomenon observed in self-field calculations for highly eccentric orbits [52,53]. Both features are associated with tail contributions to the self-field and are less visible at larger ℓ, where the "direct" part of the field is more dominant. We have not conducted here a more detailed study of the above physical features.

Finally, Fig. 10 shows the behavior of $\phi^{>}_{22}$ near $\mathcal{I}^+$, as a function of retarded time u. The periastron lag and postperiastron undulation are also visible in the radiation field in this domain.

VIII. CONCLUSION

The main results of this work are threefold. First, we have provided the details of a practical method for a time-domain calculation of the Hertz potential for point-particle metric perturbations in Schwarzschild spacetime. The main ingredients were jump conditions that the Hertz potential must satisfy along the particle's worldline (in a 1 + 1D multipolar reduction of the problem), which we derived in explicit form for generic geodesic orbits. Second, considering the numerical implementation strategy, we have demonstrated that a straightforward approach based on evolution of the Teukolsky equation in u, v coordinated does not work (even for vacuum problems) and explained the reason for that failure. Third, we have proposed a way around the problem and demonstrated its applicability with an end-to-end numerical calculation of the Hertz potential for a scatter orbit.

The specific application that motivates this work is the calculation of self-force effects on scatter orbits, and in particular the self-force correction to the scatter angle. This calculation we intend to report in forthcoming work. Let us review here the additional steps necessary toward such a calculation, starting from the baseline of the computational method and code developed here:

(i) Given the Hertz potential, the no-string radiation-gauge metric perturbation is reconstructed (mode by mode) via Eq. (7). This involves taking two derivatives of the numerical variables $\phi_{\ell m}$ (and hence four derivatives of $X_{\ell m}$) along the orbit, on either side of it. For the eventual self-force calculation, one requires the gradient of the metric perturbation, which therefore requires *three* derivatives of $\phi_{\ell m}$ (and hence *five* derivatives of $X_{\ell m}$). The computational implications are discussed further below.

(ii) One has to separately compute the "completion" piece of the metric perturbation, which is not accounted for by the Hertz potential [27,54]. In the Schwarzschild problem, this corresponds precisely to the determination of the $\ell = 0$, 1 perturbation modes. Of these, the axially symmetric modes $(l, m) = (0, 0)$ and (1,0), which describe mass and angular-momentum perturbations, are easily determinable using the results of Ref. [27]. The modes $(l, m) = (1, \pm 1)$, which regulate the center-of-mass location, require a more careful analysis, similar to the one performed in Ref. [20] for marginally bound orbits.

(iii) Once all the modes of the metric perturbation and its gradient are available, the self-force along the orbit is straightforwardly obtained via the no-string radiation-gauge version of the mode-sum formula, prescribed in Ref. [22]. It is also easy to separately extract the dissipative and conservative components of the self-force, utilizing the symmetries of the geodesic scatter orbit about the periastron point (see, e.g., Sec. 8.1 of Ref. [55]).

(iv) One can then calculate the self-force correction to the scatter angle (say, at fixed initial velocity v_∞ and impact parameter b) as certain integrals of the self-force along the orbit. The relevant formulas are straightforwardly derived from the geodesic equations with a self-force term. Additional physical quantities, such as the time delay induced by the self-force, or the integrated particle's spin precession and tidal-field invariants, may also be calculated, though the latter two would require evaluating higher derivatives of the metric perturbation. The self-force information allows calculation of all these effects with or without dissipation.

We have noted above that a calculation of the metric perturbation and self-force involves taking high-order derivatives (fourth and fifth, respectively) of the numerical evolution field $X_{\ell m}$. This is an obvious computational disadvantage of our approach. It can be mitigated if a method is employed that allows a direct evolution of the Teukolsky equation for the Hertz potential $\phi_{\ell m}$, which would reduce the required number of derivatives to only 2 for the metric perturbation and 3 for the self-force. As mentioned in Sec. V, there already exist such methods, based on compactification of $\mathcal{I}^+$ and the use of horizon-penetrating coordinates—which appear to automatically eliminate the problematic nonphysical growing solutions of the Teukolsky equation. Existing codes employ asymptotically null (hyperboloidal) Cauchy slicing of the numerical domain. We propose that, in our context, it might be advantageous to retain the convenience and simplicity of a fully double-null treatment, taking advantage of the domain split across $\mathcal{S}$. What we have in mind is a scheme where on $\mathcal{S}^+$ we use the original Eddington-Finklestein coordinate u with a compactified v coordinate, while on $\mathcal{S}^-$, we use the original v coordinate with a compactified u. The coordinate discrepancy along $\mathcal{S}$ is then incorporated into the jump conditions. We intend to explore this route in future work.

Since this work concentrates on basic method development, we have not explored in detail the performance of our code near the extremes of the parameter space for scatter orbits. Relevant asymptotic domains of interest are that of large $R_{\rm min}$ (weak-field regime) and that of large v_∞ (ultrarelativistic regime), where useful comparisons can be made with analytical approximations. Preliminary experiments suggest that, as expected, the performance of our code gradually deteriorates with larger $R_{\rm min}$ and/or larger v_∞. In large-$R_{\rm min}$ runs, we are penalized by the longer evolution time required, and in the large-v_∞ case, the slower decay of initial junk along the orbit requires a larger value of $R_{\rm init}$ (and again a longer run). We estimate, nonetheless, that our current (admittedly suboptimal) method and code can comfortably handle $R_{\rm min} \lesssim 50M$ and $v_\infty \lesssim 0.6$. Note that we virtually have no limit on how large the impact parameter b can be taken to be (indeed, in the marginally bound case studied in Ref. [20] via a similar time-domain method, one has $b \to \infty$).

It is natural to ask about the prospect of an extension to orbits in Kerr geometry. This has been discussed in some detail in Ref. [23]. A $1 + 1$D treatment of the Teukolsky equation in Kerr is still possible, albeit with the additional complication of coupling between ℓ modes. The field equation, together with jump conditions on $\mathcal{S}$, can be recast in a narrow band-diagonal matrix form and solved for all ℓ modes simultaneously (with a cutoff at a sufficiently high $\ell_{\rm max}$). The application of this mode-coupling approach has been demonstrated in vacuum problems [23,56], but it is yet to be applied with a particle source, and the appropriate no-string jump conditions are yet to be derived. In the Kerr case, there is no known way of transforming to a RW-like variable in the time domain (the Sasaki-Nakamura formulation achieves that in the frequency domain only), which further motivates an approach based on a direct evolution of the Hertz potential with a suitable form of domain compactification.

ACKNOWLEDGMENTS

We thank Gaurav Khanna for useful correspondence in relation to the issues discussed in Sec. V. O. L. acknowledges support from EPSRC through Grant No. EP/R513325/1. L. B. acknowledges support from STFC through Grant No. ST/R00045X/1. This work makes use of the Black Hole Perturbation Toolkit.

APPENDIX A: BARDEEN-PRESS-TEUKOLSKY EQUATION AND METRIC RECONSTRUCTION

We give here a more detailed technical account of the background material presented in Sec. II, and in particular, we give explicit expressions for the operators $\hat{\mathsf{T}}_\pm$, $\hat{\mathsf{O}}_\pm$, and $\hat{\mathsf{S}}_\pm$ and their adjoints. Our sign conventions for the Newman-Penrose formalism are adopted from Ref. [27]; Appendix A therein gives a useful summary.

In this paper, we use Kinnersley's null tetrad basis on a Schwarzschild background with metric $g_{\alpha\beta}$ and mass parameter M. In Schwarzschild coordinates (t, r, θ, φ), the tetrad legs are given by

$$\begin{aligned} e^\alpha_{\boldsymbol{1}} &= \ell^\alpha = \left(\frac{r^2}{\Delta}, 1, 0, 0\right), \\ e^\alpha_{\boldsymbol{2}} &= n^\alpha = \frac{1}{2}\left(1, -\frac{\Delta}{r^2}, 0, 0\right), \\ e^\alpha_{\boldsymbol{3}} &= m^\alpha = \frac{1}{\sqrt{2}r}\left(0, 0, 1, \frac{i}{\sin\theta}\right), \\ e^\alpha_{\boldsymbol{4}} &= \bar{m}^\alpha = \frac{1}{\sqrt{2}r}\left(0, 0, 1, -\frac{i}{\sin\theta}\right), \end{aligned} \tag{A1}$$

where $\Delta := r(r-2M)$ and overbars denote complex conjugation. We have $g_{\alpha\beta}e^\alpha_{\boldsymbol{a}}e^\beta_{\boldsymbol{b}} = 0$ for all $\boldsymbol{a}$ and $\boldsymbol{b}$, except $\ell^\alpha n_\alpha = -1$ and $m^\alpha \bar{m}_\alpha = 1$. The corresponding spin coefficients are $\gamma_{\boldsymbol{abc}} := g_{\mu\lambda}e^\mu_{\boldsymbol{a}}e^\nu_{\boldsymbol{c}}\nabla_\nu e^\lambda_{\boldsymbol{b}}$. Up to trivial index permutations, the only nonzero coefficients in the Schwarzschild case are

$$\begin{aligned} \varrho &:= -\gamma_{314} = -\frac{1}{r}, \\ \mu &:= -\gamma_{243} = -\frac{\Delta}{2r^3}, \\ \gamma &:= -\frac{1}{2}(\gamma_{212} + \gamma_{342}) = \frac{M}{2r^2}, \\ \beta &:= -\frac{1}{2}(\gamma_{213} + \gamma_{343}) = \frac{\cot\theta}{2\sqrt{2}r}, \\ \alpha &:= -\frac{1}{2}(\gamma_{214} + \gamma_{344}) = -\frac{\cot\theta}{2\sqrt{2}r}. \end{aligned} \tag{A2}$$

The Weyl curvature scalars Ψ_0 and Ψ_4 are defined in terms of the Weyl tensor $C_{\alpha\beta\gamma\delta}$ as

$$\begin{aligned} \Psi_0 &= C_{\alpha\beta\gamma\delta}\ell^\alpha m^\beta \ell^\gamma m^\delta, \\ \Psi_4 &= C_{\alpha\beta\gamma\delta}n^\alpha \bar{m}^\beta n^\gamma \bar{m}^\delta. \end{aligned} \tag{A3}$$

Both Ψ_0 and Ψ_4 vanish in the Schwarzschild background, and so, for the sake of economy but in a slight abuse of notation, we use these symbols to represent the linear perturbations in these quantities. We define $\Psi_+ := \Psi_0$ and $\Psi_- := \varrho^{-4}\Psi_4$ for notational ease. In terms of the metric perturbation $h_{\alpha\beta}$, we have $\hat{\mathsf{T}}_\pm h_{\alpha\beta} = \Psi_\pm$ [Eq. (2)], where the second-order differential operators $\hat{\mathsf{T}}_\pm$ are given by

$$\begin{aligned} (\hat{\mathsf{T}}_+)^{\alpha\beta} &= \frac{1}{2}(\ell^{(\alpha}m^{\beta)}m^\gamma\ell^\delta - m^\alpha m^\beta \ell^\gamma \ell^\delta - \ell^\alpha \ell^\beta m^\gamma m^\delta, \\ &\quad + m^{(\alpha}\ell^{\beta)}\ell^\gamma m^\delta)\nabla_\delta\nabla_\gamma, \\ (\hat{\mathsf{T}}_-)^{\alpha\beta} &= \frac{1}{2}(n^{(\alpha}\bar{m}^{\beta)}\bar{m}^\gamma n^\delta - \bar{m}^\alpha\bar{m}^\beta n^\gamma n^\delta - n^\alpha n^\beta \bar{m}^\gamma \bar{m}^\delta \\ &\quad + \bar{m}^{(\alpha}n^{\beta)}n^\gamma\bar{m}^\delta)\nabla_\delta\nabla_\gamma. \end{aligned} \tag{A4}$$

Here, ∇_α is the covariant derivative compatible with the Schwarzschild background metric $g_{\alpha\beta}$, and parenthetical indices are symmetrized, as in $A_{(\alpha\beta)} = \frac{1}{2}(A_{\alpha\beta} + A_{\beta\alpha})$.

The perturbation fields $\Psi_\pm$ satisfy the Teukolsky equation with spin parameter $s = \pm 2$, whose Schwarzschild reduction is sometimes referred to as the Bardeen-Press equation. Here, we refer to it as the Bardeen-Press-Teukolsky equation. It has the form

$$\hat{\mathsf{O}}_\pm \Psi_\pm = \mathcal{T}_\pm, \tag{A5}$$

where the differential operators on the left are

$$\begin{aligned} \hat{\mathsf{O}}_+ &= \Delta\left(\boldsymbol{D}_\ell + 2\frac{r-M}{\Delta}\right)\left(\tilde{\boldsymbol{D}}_n + 4\frac{r-M}{\Delta}\right) + \eth_1\bar{\eth}_2 - 6r\partial_t, \\ \hat{\mathsf{O}}_- &= \Delta\left(\tilde{\boldsymbol{D}}_n - 2\frac{r-M}{\Delta}\right)\boldsymbol{D}_\ell + \bar{\eth}_{-1}\eth_{-2} + 6r\partial_t. \end{aligned} \tag{A6}$$

Here, $\boldsymbol{D}_\ell := \ell^\alpha\nabla_\alpha$, $\boldsymbol{D}_n := n^\alpha\nabla_\alpha$, $\tilde{\boldsymbol{D}}_n := -(2r^2/\Delta)\boldsymbol{D}_n$, and we have introduced the "spin raising and lowering" operators, respectively,

$$\begin{aligned} \eth_s &:= -\partial_\theta - i\csc\theta\partial_\varphi + s\cot\theta, \\ \bar{\eth}_s &:= -\partial_\theta + i\csc\theta\partial_\varphi - s\cot\theta, \end{aligned} \tag{A7}$$

whose action on spin-weighted spherical harmonics ${}_sY_{\ell m}(\theta, \varphi)$ is described by

$$\begin{aligned} \eth_s {}_sY_{\ell m} &= +\sqrt{(\ell - s)(\ell + s + 1)}\,{}_{s+1}Y_{\ell m}, \\ \bar{\eth}_s {}_sY_{\ell m} &= -\sqrt{(\ell + s)(\ell - s + 1)}\,{}_{s-1}Y_{\ell m}. \end{aligned} \tag{A8}$$

The source terms $\mathcal{T}_\pm$ in (A5) are obtained from the energy-momentum tensor $T_{\alpha\beta}$ using

$$\begin{aligned}\mathcal{T}_+ = \hat{\mathsf{S}}_+ T_{\alpha\beta} = 8\pi r^2 \\ \times [(\boldsymbol{D}_m - 2\beta)\boldsymbol{D}_m T_{\mathbf{11}} - (\boldsymbol{D}_\ell - 5\varrho)(\boldsymbol{D}_m - 2\beta)T_{\mathbf{13}} \\ - (\boldsymbol{D}_m - 2\beta)(\boldsymbol{D}_\ell - 2\varrho)T_{\mathbf{13}} + (\boldsymbol{D}_\ell - 5\varrho)(\boldsymbol{D}_\ell - \varrho)T_{\mathbf{33}}],\end{aligned} \tag{A9}$$

$$\begin{aligned}\mathcal{T}_- = \hat{\mathsf{S}}_- T_{\alpha\beta} = 8\pi r^6 \\ \times [(\boldsymbol{D}_{\bar{m}} - 2\beta)\boldsymbol{D}_{\bar{m}} T_{\mathbf{22}} - (\boldsymbol{D}_n + 2\gamma + 5\mu)(\boldsymbol{D}_{\bar{m}} - 2\beta)T_{\mathbf{24}} \\ - (\boldsymbol{D}_{\bar{m}} - 2\beta)(\boldsymbol{D}_n + 2\gamma + 2\mu)T_{\mathbf{24}} \\ + (\boldsymbol{D}_n + 2\gamma + 5\mu)(\boldsymbol{D}_n + \mu)T_{\mathbf{44}}],\end{aligned} \tag{A10}$$

where $T_{\mathbf{11}} = T_{\alpha\beta}e_1^\alpha e_1^\beta$, etc., and we have also introduced $\boldsymbol{D}_m \coloneqq m^\alpha \nabla_\alpha$ and $\boldsymbol{D}_{\bar{m}} \coloneqq \bar{m}^\alpha \nabla_\alpha$,

As described in Sec. II, the metric reconstruction procedure involves the operators adjoint to $\hat{\mathsf{O}}_+$, $\hat{\mathsf{T}}_+$, and $\hat{\mathsf{S}}_+$. These adjoint operators can be obtained by integrating each operator against a suitable test function and manipulating using integrations by parts. In this fashion, it is straightforward to show that

$$\hat{\mathsf{O}}_\pm^\dagger = \hat{\mathsf{O}}_\mp; \tag{A11}$$

i.e., solutions $\Phi_\pm$ to the adjoint BPT equation with spin $s = \pm 2$ are also solutions to the standard BPT equation with spin $s = \mp 2$. For the metric reconstruction operators [see Eq. (7)], a calculation gives

$$\begin{aligned}\hat{S}_+^\dagger = -2\ell_\alpha \ell_\beta (\boldsymbol{D}_m + 2\beta)(\boldsymbol{D}_m + 4\beta) \\ - 2\ell_{(\alpha} m_{\beta)}[(\boldsymbol{D}_m + 4\beta)(\boldsymbol{D}_\ell + 3\varrho) + \boldsymbol{D}_\ell(\boldsymbol{D}_m + 4\beta)] \\ + 2m_\alpha m_\beta(\boldsymbol{D}_\ell - \varrho)(\boldsymbol{D}_\ell + 3\varrho),\end{aligned} \tag{A12}$$

$$\begin{aligned}\hat{S}_-^\dagger = -2r^4[n_\alpha n_\beta(\boldsymbol{D}_{\bar{m}} + 2\beta)(\boldsymbol{D}_{\bar{m}} + 4\beta) \\ - n_{(\alpha}\bar{m}_{\beta)}((\boldsymbol{D}_{\bar{m}} + 4\beta)(\boldsymbol{D}_n + \mu - 4\gamma) \\ + (\boldsymbol{D}_n + 4\mu - 4\gamma)(\boldsymbol{D}_{\bar{m}} - 2\beta)) \\ + \bar{m}_\alpha \bar{m}_\beta(\boldsymbol{D}_n + 5\mu - 2\gamma)(\boldsymbol{D}_n + \mu - 4\gamma)].\end{aligned} \tag{A13}$$

Finally, for the “source reconstruction” operators [see Eq. (15)], one finds

$$\begin{aligned}(\hat{\mathsf{T}}_+^\dagger)^{\alpha\beta} = -\frac{1}{2}\ell^\alpha \ell^\beta(\boldsymbol{D}_m + 2\beta)(\boldsymbol{D}_m + 4\beta) \\ + \frac{1}{2}\ell^{(\alpha}m^{\beta)}[\boldsymbol{D}_\ell(\boldsymbol{D}_m + 4\beta) + (\boldsymbol{D}_m + 4\beta)(\boldsymbol{D}_\ell - \varrho)] \\ - \frac{1}{2}m^\alpha m^\beta(\boldsymbol{D}_\ell - \varrho)^2,\end{aligned} \tag{A14}$$

$$\begin{aligned}(\hat{\mathsf{T}}_-^\dagger)^{\alpha\beta} = -\frac{1}{2}n^\alpha n^\beta(\boldsymbol{D}_{\bar{m}} + 2\beta)(\boldsymbol{D}_{\bar{m}} + 4\beta) \\ + \frac{1}{2}n^{(\alpha}\bar{m}^{\beta)}[(\boldsymbol{D}_n - 4\gamma)(\boldsymbol{D}_{\bar{m}} + 4\beta) \\ + (\boldsymbol{D}_{\bar{m}} + 4\beta)(\boldsymbol{D}_n + \mu - 4\gamma)] \\ - \frac{1}{2}\bar{m}^\alpha \bar{m}^\beta(\boldsymbol{D}_n + \mu - 2\gamma)(\boldsymbol{D}_n + \mu - 4\gamma).\end{aligned} \tag{A15}$$

APPENDIX B: JUMPS IN THE WEYL-SCALAR MODES $\psi_{\ell m}^\pm$

In this Appendix, we derive the jumps across $\mathcal{S}$ in the Weyl-scalar modal fields $\psi_{\ell m}^\pm(t,r)$ and their first three derivatives, for a generic geodesic orbit. We do so analytically, and for both spins $s = \pm 2$. These jumps are necessary input for the calculation of the no-string Hertz-potential jumps $[\phi_\pm]$ in Sec. IV. In our method, we require both $[\psi_+]$ and $[\psi_-]$ for either $[\phi_+]$ (IRG potential) or $[\phi_-]$ (ORG potential); cf. Eq. (60) with (61). At the end of this Appendix, we derive asymptotic expressions for $[\psi_\pm]$ at large radii in the case of scatter orbits; these are used in the asymptotic analysis of Sec. IV C.

1. BPT equation with a point-particle source

Let $\Psi_+ \equiv \Psi_0$ and $\Psi_- \equiv r^4\Psi_4$ be the Weyl scalars associated with the physical metric perturbation sourced by a geodesic point particle with stress-energy as in Eq. (16). We recall our notation: μ is the particle's mass, and $x^\mu = x_p^\mu(\tau)$ describes its geodesic worldline, with proper time τ and 4-velocity $u^\alpha \coloneqq dx_p/d\tau$. For convenience, we set the Schwarzschild coordinates so that the orbit lies in the equatorial plane ($\theta_p \equiv \pi/2$) and write $R(\tau) \equiv r_p(\tau)$. The conserved (specific) energy and angular momentum of the orbit are $E = f_R u^t$ and $L = r^2 u^\varphi$, respectively, where $f_R \coloneqq 1 - 2M/R$. The Schwarzschild components of the 4-velocity are

$$u_p^\mu = (E/f_R, (E/f_R)\dot{R}, 0, L/r^2), \tag{B1}$$

where an overdot denotes d/dt.

The Weyl scalars $\Psi_\pm$ satisfy the $s = \pm 2$ BPT equations (A5), where the source $\mathcal{T}_\pm$ is derivable from $T^{\alpha\beta}$ by means of Eqs. (A9) and (A10). Expanding both $\Psi_\pm$ and $\mathcal{T}_\pm$ in $s = \pm 2$ spherical harmonics, as in Eq. (24), separates the BPT equation into modal equations for each of the time-radial fields $\psi_{\ell m}^\pm(t,r)$. The modal equations are (dropping the indices ℓm for brevity)

$$\psi_{,uv}^\pm + U_s(r)\psi_{,u}^\pm + V_s(r)\psi_{,v}^\pm + W_s(r)\psi^\pm = T_\pm(t,r), \tag{B2}$$

where the radial functions on the left are those given in Eqs. (26) and (27), with $s = \pm 2$ for $\psi_\pm$. The modal source term $T_\pm$ can be written in the form

$$T_{\pm}(t,r) = s_0^{\pm}(t)\delta[r-R(t)] + s_1^{\pm}(t)\delta'[r-R(t)] + s_2^{\pm}(t)\delta''[r-R(t)], \tag{B3}$$

where a prime denotes a derivative with respect to the argument, and the source functions $s_n^{\pm}(t)$ are certain functions along the orbit. The explicit expressions for $s_n^{\pm}(t)$ are rather unwieldy, unfortunately, but they are essential within our method, so we give them here. They are

$$\begin{aligned} s_0^+ = \frac{\pi\mu}{E}\{&-L^2 m f_R^2 R(i\ddot{\varphi}_p + m\dot{\varphi}_p^2) + 2Lf_R[iLm((2+y)f_R - (1+2y)\dot{R}) + m^2 ER(f_R - \dot{R})]\dot{\varphi}_p \\ &+ Lf_R[L(1+2y) - 2imER]\ddot{R} + [-2iLEm + 8L^2y^2/R - (m^2-2)E^2R]\dot{R}^2 \\ &+ 2f_R[-(L^2/R)y(6y+7) + 2iLmE(1+3y) + (m^2-2)E^2R]\dot{R} + 12f_R^2(L^2/R)y \\ &- f_R^2[2iLmE(1+4y) + (m^2-2)E^2R]\}\mathcal{Y}^+(t) + \pi\mu\{2R(f_R-\dot{R})m[Lf_R\dot{\varphi}_p - E(f_R-\dot{R})] \\ &+ 2iL[-f_R R\ddot{R} - \dot{R}^2 + 2f_R(1+3y)\dot{R} - f_R^2(1+4y)]\}\mathcal{Y}_\theta^+(t) - \pi\mu ER(f_R-\dot{R})^2\mathcal{Y}_{\theta\theta}^+(t), \end{aligned} \tag{B4}$$

$$\begin{aligned} s_1^+ = {}& 2i\pi\mu L f_R R(f_R-\dot{R})[(f_R-\dot{R})[\mathcal{Y}_\theta^+(t) + m\mathcal{Y}^+(t)] - mf_R(L/E)\dot{\varphi}_p\mathcal{Y}^+(t)] + \pi\mu(L^2/E)f_R[-f_R R\ddot{R} - 2(1+2y)\dot{R}^2 \\ &+ 2f_R(3+5y)\dot{R} - 4f_R^2(1+y)]\mathcal{Y}^+(t), \end{aligned} \tag{B5}$$

$$s_2^+ = \pi\mu(L^2/E)f_R^2 R(f_R-\dot{R})^2\mathcal{Y}^+(t), \tag{B6}$$

and

$$\begin{aligned} s_0^- = -\frac{\pi\mu}{4Ef_R^2R^9}\{&L^2 m f_R^2 R^6(m\dot{\varphi}_p^2 + i\ddot{\varphi}_p) - 2LmR^5 f_R[EmR\dot{R} + f_R(EmR + iL(3\dot{R} + 2 - 5y))]\dot{\varphi}_p \\ &+ Lf_R R^5(3Lf_R - 2iEmR)\ddot{R} + R^4[-12L^2f_R^2 + ER(E(m^2-2)R + 2iLm(3-4y))]\dot{R}^2 \\ &+ 2R^4[-L^2(8-25y)f_R^2 + ER(E(m^2-2)Rf_R + 2iLm(3-7y)f_R)]\dot{R} \\ &+ R^4[-4L^2(1-5y)f_R^3 + ER(E(m^2-2)Rf_R^2 + 2iLm(3-8y)f_R^2)]\}\mathcal{Y}^-(t) \\ &+ \frac{\pi\mu}{2f_R^2R^7}\{mR^4(f_R+\dot{R})(E(f_R+\dot{R}) - Lf_R\dot{\varphi}_p) - iLR^3(f_R R\ddot{R} - (3-4y)\dot{R}^2 - 2f_R(3-7y)\dot{R} \\ &- (3-8y)f_R^2)\}\mathcal{Y}_\theta^-(t) - \frac{\pi E\mu(f_R+\dot{R})^2}{4f_R^2R^3}\mathcal{Y}_{\theta\theta}^-(t), \end{aligned} \tag{B7}$$

$$\begin{aligned} s_1^- = {}& \frac{i\pi\mu L(f_R+\dot{R})}{2f_R R^3}[(f_R+\dot{R})[\mathcal{Y}_\theta^-(t) - m\mathcal{Y}^-(t)] \\ &+ mf_R(L/E)\dot{\varphi}_p\mathcal{Y}^-(t)] + \frac{\pi\mu L^2}{4ER^4}[-R\ddot{R} + 6\dot{R}^2 \\ &+ 2(5-13y)\dot{R} + 4f_R(1-3y)]\mathcal{Y}^-(t), \end{aligned} \tag{B8}$$

$$s_2^- = \frac{\pi\mu L^2(f_R+\dot{R})^2}{4ER^3}\mathcal{Y}^-(t). \tag{B9}$$

Here, we have introduced

$$y \coloneqq \frac{M}{R}, \qquad \mathcal{Y}^{\pm}(t) \coloneqq {}_{\pm 2}\bar{Y}_{\ell m}\left(\frac{\pi}{2}, \varphi_p(t)\right), \tag{B10}$$

with $\mathcal{Y}_\theta^{\pm}$ and $\mathcal{Y}_{\theta\theta}^{\pm}$ being the first and second derivatives of ${}_{\pm 2}\bar{Y}_{\ell m}(\theta, \varphi_p(t))$ with respect to θ, evaluated at $\theta = \pi/2$.

Note that in Eqs. (B4)–(B9) we have not yet specialized to a timelike geodesic. With such specification, the time derivatives featuring in these expressions can be expressed in terms of $R(t)$ alone (as well as E and L), as follows:

$$\dot{R} = \pm(f_R/E)[E^2 - f_R(1 + L^2/R^2)]^{1/2}, \tag{B11}$$

$$\ddot{R} = \frac{f_R^2(1-5y)L^2 + yR^2 f_R(2E^2 - 3f_R)}{R^3E^2}, \tag{B12}$$

$$\dot{\varphi}_p = \frac{f_R L}{R^2 E}, \qquad \ddot{\varphi}_p = -\frac{2L(1-3y)\dot{R}}{ER^3}. \tag{B13}$$

The sign in (B11) is (−) for the incoming leg of the orbit and (+) for the outgoing leg.

2. Jumps in $\psi_\pm$ and their first derivatives

The jumps in the $1+1$D Weyl-scalar fields $\psi_\pm$ are determined by requiring that (B2) is satisfied as a distributional equation, with the ansatz

$$\psi_\pm = \psi^>_\pm(t,r)\Theta[r-R(t)] + \psi^<_\pm(t,r)\Theta[R(t)-r] + \psi^\pm_\delta(t)\delta[r-R(t)]. \tag{B14}$$

Here, $\Theta[\cdot]$ is the Heaviside step function, and $\psi^\pm_\delta(t)$ is to be determined. Balancing the coefficients of $\Theta[r-R(t)]$ and $\Theta[R(t)-r]$ implies that $\psi^>_\pm(t,r)$ and $\psi^<_\pm(t,r)$ are homogeneous solutions of (B2). The remaining terms are supported on $r=R(t)$ only and are each proportional to either δ, δ', or δ''. We use the distributional identities

$$\begin{aligned}F(r)\delta(r-R) &= F(R)\delta(r-R),\\ F(r)\delta'(r-R) &= F(R)\delta'(r-R) - F'(R)\delta(r-R),\\ F(r)\delta''(r-R) &= F(R)\delta''(r-R) - 2F'(R)\delta'(r-R)\\ &\quad + F''(R)\delta(r-R)\end{aligned} \tag{B15}$$

[valid for any smooth function $F(r)$] to eliminate the r dependence of the coefficients of each of these terms and then compare the coefficient values across the two sides of Eq. (B2), recalling the form of $T_\pm$ in Eq. (B3).

From the coefficient of δ'', we immediately obtain

$$\psi^\pm_\delta(t) = -\frac{4s^\pm_2(t)}{f_R^2-\dot{R}^2}. \tag{B16}$$

The coefficient of δ' then determines the jump,

$$\begin{aligned}[\psi_\pm] = -\frac{1}{f_R^2-\dot{R}^2}\Big\{&4s_1(t) + 2\dot{\psi}^\pm_\delta \dot{R}\\ &+ [-2f_R(s(1-y)+3y) + 2s(1-3y)\dot{R} + R\ddot{R}]\frac{\psi^\pm_\delta}{R}\Big\},\end{aligned} \tag{B17}$$

with $s=\pm2$ for $\psi_\pm$. Finally, comparing the coefficients of δ gives a relation between the jumps $[\psi^\pm_{,t}]$ and $[\psi^\pm_{,r}]$:

$$s^\pm_0(t) = -\frac{1}{2}\dot{R}[\psi^\pm_{,t}] - \frac{1}{4}(f_R^2+\dot{R}^2)[\psi^\pm_{,r}] + P_\pm(t), \tag{B18}$$

where

$$\begin{aligned}P_\pm = {}&\frac{1}{4}\ddot{\psi}^\pm_\delta + \frac{s}{2R}(1-3y)\dot{\psi}^\pm_\delta\\ &+ \frac{\psi^\pm_\delta}{4R^2}[\lambda f_R + 2 + s - s^2 + 2y(1+s^2-4s)\\ &+ 8y^2(s-2) - 2s(1-6y)\dot{R}]\\ &+ \frac{[\psi_\pm]}{4R}[2f_R(s(1-y)+y) - 2s(1-3y)\dot{R} - R\ddot{R}],\end{aligned} \tag{B19}$$

with $s=\pm2$ for $P_\pm$. Recall $\lambda=(l+2)(l-1)$.

A second relation between $[\psi^\pm_{,t}]$ and $[\psi^\pm_{,r}]$ is obtained by writing

$$[\dot{\psi}_\pm] = [\psi^\pm_{,t}] + \dot{R}[\psi^\pm_{,r}]. \tag{B20}$$

Solving (B18) and (B20) as a simultaneous set then gives

$$[\psi^\pm_{,r}] = \frac{4(P_\pm - s^\pm_0) - 2\dot{R}[\dot{\psi}_\pm]}{f_R^2-\dot{R}^2}, \tag{B21}$$

and

$$[\psi^\pm_{,t}] = \frac{-4(P_\pm - s^\pm_0)\dot{R} + (f_R^2+\dot{R}^2)[\dot{\psi}_\pm]}{f_R^2-\dot{R}^2}. \tag{B22}$$

The corresponding jumps in the u and v derivatives are

$$[\psi^\pm_{,v}] = \frac{4(P_\pm - s^\pm_0) + (f_R-\dot{R})[\dot{\psi}_\pm]}{2(f_R+\dot{R})}, \tag{B23}$$

$$[\psi^\pm_{,u}] = \frac{-4(P_\pm - s^\pm_0) + (f_R+\dot{R})[\dot{\psi}_\pm]}{2(f_R-\dot{R})}. \tag{B24}$$

Equations (B17), (B23), and (B24) give the jumps in $\psi_\pm$ and its first derivatives for a generic geodesic orbit.

3. Jumps in the second and third derivatives of $\psi_\pm$

We can get $[\psi^\pm_{,uv}]$ directly from the vacuum BPT equation,

$$[\psi^\pm_{,uv}] = -U_{\pm2}(R)[\psi^\pm_{,u}] - V_{\pm2}(R)[\psi^\pm_{,v}] - W_{\pm2}(R)[\psi_\pm], \tag{B25}$$

where the jumps $[\psi^\pm_{,v}]$, $[\psi^\pm_{,u}]$ and $[\psi^\pm]$ can be substituted for from Eqs. (B23), (B24), and (B17). Then, $[\psi^\pm_{,uu}]$ and $[\psi^\pm_{,vv}]$ can be obtained from the chain rules

$$\begin{aligned}[\dot{\psi}^\pm_{,u}] &= \dot{v}[\psi^\pm_{,uv}] + \dot{u}[\psi^\pm_{,uu}],\\ [\dot{\psi}^\pm_{,v}] &= \dot{v}[\psi^\pm_{,vv}] + \dot{u}[\psi^\pm_{,uv}],\end{aligned} \tag{B26}$$

where

$$\dot{v} = 1 + \dot{R}/f_R, \qquad \dot{u} = 1 - \dot{R}/f_R. \tag{B27}$$

The jumps in the third derivatives are obtained in a similar fashion. First, we obtain $[\psi^{\pm}_{,uvu}]$ and $[\psi^{\pm}_{,uvv}]$ from the u and v derivatives of the vacuum BPT equations. Then, $[\psi^{\pm}_{,uuu}]$ and $[\psi^{\pm}_{,vvv}]$ are determined from the appropriate chain rule; e.g.,

$$[\psi^{\pm}_{,uuu}] = \frac{[\dot{\psi}^{\pm}_{uu}] - \dot{v}[\psi^{\pm}_{,uuv}]}{\dot{u}}, \tag{B28}$$

where the jumps on the right-hand side are known from previous steps. We may proceed in this recursive manner to determine the jumps in all higher derivatives. In the calculation performed in this paper, we require jump information only up to the third derivatives.

4. Large-R asymptotics for scatter orbits

For our asymptotic analysis in Sec. IV C (where we derive initial conditions for the Hertz potential's jump equations), it is useful to have at hand the large-R asymptotic form of the Weyl-scalar jumps calculated above, in the case of a scatter orbit coming from infinity (i.e., the class of geodesic scatter orbits described in Sec. VII A). Specifically, we need the asymptotic forms of $[\psi_{\pm}]$ as well as $[\psi^{+}_{,u}]$, $[\psi^{+}_{,uu}]$, and $[\psi^{+}_{,uuu}]$.

As input for this calculation, we need the asymptotic form of the source coefficients $s^{\pm}_n$ in Eqs. (B4)–(B9). Specializing to scatter geodesics and working at leading order in $y = M/R$ (at fixed E, L), we find

$$\begin{aligned} s^{+}_n &= \sigma^{+}_n R + O(R^0), \\ s^{-}_n &= \sigma^{-}_n R^{-3} + O(R^{-4}), \end{aligned} \tag{B29}$$

for $n = 0, 1, 2$. The coefficients needed for our purpose are given explicitly by

$$\begin{aligned} \sigma^{+}_0 &= -\mu E \pi (1 - \dot{R}_\infty)^2 [(m^2 - 2)\mathcal{Y}^{+} + 2m\mathcal{Y}^{+}_{\theta} + \mathcal{Y}^{+}_{\theta\theta}]_\infty, \\ \sigma^{+}_1 &= \mp 2i\mu L \pi (1 - \dot{R}_\infty)^2 (m\mathcal{Y}^{+} + \mathcal{Y}^{+}_{\theta})_\infty, \end{aligned} \tag{B30}$$

and

$$\sigma^{-}_1 = \pm \frac{1}{2} i\mu L (1 + \dot{R}_\infty)^2 (m\mathcal{Y}^{-} - \mathcal{Y}^{-}_{\theta})_\infty, \tag{B31}$$

where subscripts ∞ imply an evaluation at $t \to \pm\infty$, depending on whether it is the in or out states being considered. In the expressions for σ^{+}_1 and σ^{-}_1, the upper sign is for the out state ($\dot{R}_\infty > 0$), and the lower sign is for the in state ($\dot{R}_\infty < 0$).

A straightforward leading-order calculation now gives

$$[\psi_{+}] = -4\sigma^{+}_1 E^2 R + O(R^0), \tag{B32}$$

$$[\psi_{-}] = -4\sigma^{-}_1 E^2 R^{-3} + O(R^{-4}), \tag{B33}$$

as well as

$$[\psi^{+}_{,t}] = -\dot{R}_\infty [\psi^{+}_{,r}] = 4\sigma^{+}_0 E^2 \dot{R}_\infty R + O(R^0), \tag{B34}$$

$$[\psi^{+}_{,u}] = \frac{2\sigma^{+}_0}{1 - \dot{R}_\infty} R + \mathcal{O}(R^0), \tag{B35}$$

$$[\psi^{+}_{,uu}] = -\frac{2\sigma^{+}_0 (2 - 3\dot{R}_\infty)}{(1 - \dot{R}_\infty)^2} + \mathcal{O}(R^{-1}), \tag{B36}$$

$$[\psi^{+}_{,uuu}] = \frac{\sigma^{+}_0 [8(1 - 2\dot{R}_\infty) + \lambda(1 + \dot{R}_\infty)]}{2(1 - \dot{R}_\infty)^2} R^{-1} + O(R^{-2}). \tag{B37}$$

APPENDIX C: FINITE-DIFFERENCE SCHEME

In this Appendix, we detail the finite-difference (FD) scheme employed in Sec. VII for solving the $1 + 1$D vacuum RW field equation (75), with jump conditions on $\mathcal{S}$ corresponding to a no-string Hertz potential for a scatter orbit. The basic architecture of our characteristic evolution scheme was described in Sec. V A. Here, we focus on the FD scheme itself, at the grid-cell level. In deriving the scheme, we follow the method of Ref. [41] (which itself builds on a long history of time-domain work in the self-force literature, e.g., Refs. [38,57]).

Recall Fig. 1, which shows the $1 + 1$D numerical grid, based on u, v coordinates with uniform cell dimensions $h \times h$. Consider an arbitrary grid point c with coordinates $(u, v) = (u_c, v_c)$, and in reference to that point denote by X_{nk} the value of the numerical field variable X at the grid point with coordinates $(u, v) = (u_c - nh, v_c - kh)$. Our goal is to prescribe a FD expression for X_{00} (the field at c), given the values X_{nk} for all $n, k > 0$, assumed to have been obtained in previous steps of the characteristic evolution. We wish to achieve a global quadratic convergence, i.e., an accumulated error in X that scales as h^2. Since the total number of grid points over which the error accumulates is $\propto h^{-2}$, this demands a local (single-point) FD error not larger than $O(h^4)$ in general.

Our grid is traversed by the curve $\mathcal{S}$ representing the timelike geodesic trajectory of the particle. The curve is fixed and known in advance, and the coordinates of all of its intersections with grid lines are calculated in advance of the numerical evolution. In reference to the grid cell C with top vertex c, we distinguish between two scenarios: either C is traversed by $\mathcal{S}$ ("particle cell") or it is not ("vacuum cell"). We deal with each of these two scenarios separately below.

1. Vacuum cells

First, we consider the simpler case where the particle's worldline does not cross the integration cell. Then, a sufficiently accurate FD approximation for X_{00} can be written based on the three values X_{01}, X_{10}, and X_{11} alone: integrating each of the two terms on the left-hand side of the RW equation (75) over the grid cell C, we have

$$\int_C X_{,uv}du dv = X_{00} - X_{01} - X_{10} + X_{11} \qquad \text{(C1)}$$

(exactly) and

$$\int_C \mathcal{W}(r)X du dv = \frac{1}{2}h^2\mathcal{W}(r_c)(X_{01}+X_{10}) + O(h^4), \qquad \text{(C2)}$$

where

$$\mathcal{W}(r) := \frac{f}{4}\left(\frac{\lambda_1}{r^2} - \frac{6M}{r^3}\right), \qquad \text{(C3)}$$

and r_c is the value of r at point c. The vacuum RW equation then gives

$$X_{00} = -X_{11} + (X_{01}+X_{10})\left(1 - \frac{h^2}{2}\mathcal{W}(r_c)\right) + O(h^4), \qquad \text{(C4)}$$

which we use as our FD formula for vacuum points.

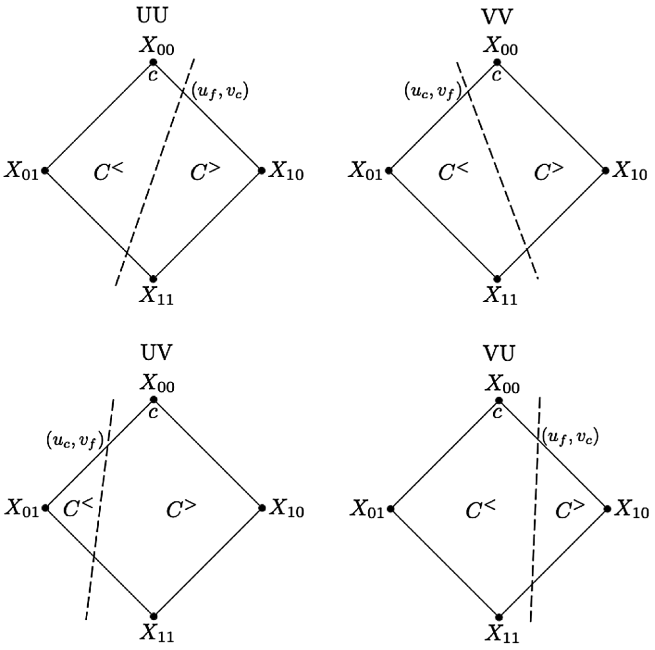

FIG. 11. A particle cell is traversed by the particle's worldline (dashed curve) in one of four possible ways: cases UU, VV, UV, and VU, illustrated here. A different variant of the FD formula applies in each case, as described in the text. The apex of the cell is the point c at $(u,v)=(u_c,v_c)$, and the particle exits the cell at (u_f,v_c) or (u_c,v_f), depending on the case. The vacuum portions of the cell left and right of the worldline are $C^<$ and $C^>$, respectively.

2. Particle cells

The vacuum formula (C4) does not work for cells that are traversed by the worldline, due to the discontinuity in the field across $\mathcal{S}$. The worldline splits C into two disjoint vacuum regions, $C^>$ and $C^<$, as shown in Fig. 11, which displays the four possible scenarios. Since X is smooth on each of the two vacuum regions, we can expand it piecewise in a Taylor series about point c, in the form

$$X^{\gtrless} = \sum_{i+j=0}^{N} \frac{c_{ij}^{\gtrless}}{i!j!}\tilde{u}^i\tilde{v}^j + O(h^{N+1}), \qquad \text{(C5)}$$

where $\tilde{u} := u - u_c$, $\tilde{v} := v - v_c$, and different expansion coefficients apply on each side of $\mathcal{S}$: $c_{ij}^<$ are used in $C^<$, and $c_{ij}^>$ are used in $C^>$. The idea now is to derive the values of $c_{ij}^{\gtrless}$ based on a sufficient number of data points $X_{nk}^{\gtrless}$, plus the analytically known jumps in X and its derivatives on $\mathcal{S}$. We note that, since the total number of particle cells scales as h^{-1}, it is acceptable for our local FD scheme to have an error as great as $O(h^3)$ (but not greater) at each particle cell.

To achieve such accuracy we take $N=2$ in Eq. (C5), leaving us with 12 coefficients $c_{ij}^{\gtrless}$ to determine. We use the six data points $\{X_{00}, X_{01}, X_{10}, X_{11}, X_{02}, X_{20}\}$ to supply six constraints, and six additional constraints are obtained from the known jumps $\{[X], [X_{,u}], [X_{,v}], [X_{,uu}], [X_{,uv}], [X_{,vv}]\}$, imposed at the point where the worldline exits the cell C [i.e., referring to Fig. 11, either the point (u_f, v_c) or the point (u_c, v_f), depending on the case]. For example, in cases UU and VU, we have the constraint

$$[X]_{(u_f,v_c)} = \sum_{i=0}^{2} \frac{(c_{i0}^> - c_{i0}^<)}{i!}\tilde{u}_f^i + O(h^3), \qquad \text{(C6)}$$

where $\tilde{u}_f = u_f - u_c$. Solving the 12 simultaneous equations for $c_{ij}^{\gtrless}$ and then substituting these coefficients back in (C5) gives an expression for $X^{\gtrless}$, accurate through $O(h^2)$ in the vicinity of point c [i.e., with an error $O(h^3)$], in terms of the above six field points (which include the unknown X_{00}) and above six jumps.

Considering first the principal part of the RW equation, we thus obtain

$$\begin{aligned} X_{,uv}^{\gtrless} &= c_{11}^{\gtrless} + O(h) \\ &= h^{-2}(X_{00} - X_{01} - X_{10} + X_{11} + J_1^A) + O(h), \end{aligned} \qquad \text{(C7)}$$

where $A \in \{UU, VV, UV, VU\}$ labels the case in question, with

$$
\begin{aligned}
J_1^{UU} &= h[X_{,v}] + h(u_c - u_f)[X_{,uv}] - \frac{h^2}{2}(2[X_{,uv}] + [X_{,vv}]),\\
J_1^{VV} &= -h[X_{,u}] - h(v_c - v_f)[X_{,uv}] + \frac{h^2}{2}(2[X_{,uv}] + [X_{,uu}]),\\
J_1^{UV} &= -[X] + (h - v_c + v_f)[X_{,v}] - \frac{1}{2}(h - v_c + v_f)^2[X_{,vv}],\\
J_1^{VU} &= [X] - (h - u_c + u_f)[X_{,u}] + \frac{1}{2}(h - u_c + u_f)^2[X_{,uu}].
\end{aligned} \tag{C8}
$$

For the term $\mathcal{W}X$ of the RW equation, we wish to obtain a FD approximation that does not involve X_{00}, and the form of (C7) implies that we only require a leading-order, $O(h^0)$ approximation for this term. We choose to achieve this by taking $N = 1$ in Eq. (C5) and then solving for the six coefficients $c_{ij}^{\gtrless}$ $(i + j \leq 1)$ using the three data points $\{X_{01}, X_{10}, X_{11}\}$ and three jumps $\{[X], [X_{,u}], [X_{,v}]\}$, again evaluated at (u_f, v_c) or (u_c, v_f). This gives

$$
\begin{aligned}
X^{\gtrless} &= c_{00}^{\gtrless} + O(h)\\
&= X_{01} + X_{10} - X_{11} + J_2^A + O(h),
\end{aligned} \tag{C9}
$$

with

$$
J_2^{UU} = 0 = J_2^{VV}, \qquad J_2^{\mathrm{UV}} = [X] = -J_2^{VU}. \tag{C10}
$$

Hence,

$$
\mathcal{W}X^{\gtrless} = \mathcal{W}(r_c)(X_{01} + X_{10} - X_{11} + J_2^A) + O(h). \tag{C11}
$$

Imposing finally the vacuum RW equation $X_{,uv} + \mathcal{W}X = 0$, we obtain, using (C7) and (C11),

$$
\begin{aligned}
X_{00} = {}& (X_{01} + X_{10} - X_{11})(1 - h^2\mathcal{W}(r_c)) - J_1^A\\
& - h^2\mathcal{W}(r_c)J_2^A + O(h^3),
\end{aligned} \tag{C12}
$$

which is our FD formula for particle cells.

Note that our second-order-convergent FD scheme, consisting of Eq. (C4) for vacuum cells with Eq. (C12) for particle cells, requires as input only the three field data points X_{01}, X_{10}, and X_{11} (as well as the known jumps). This is convenient, as it means that at each characteristic evolution step we require data on a single previously calculated characteristic ray.

[1] T. Damour, Gravitational scattering, post-Minkowskian approximation and effective one-body theory, Phys. Rev. D **94**, 104015 (2016).

[2] T. Damour, High-energy gravitational scattering and the general relativistic two-body problem, Phys. Rev. D **97**, 044038 (2018).

[3] T. Damour, Classical and quantum scattering in post-Minkowskian gravity, Phys. Rev. D **102**, 024060 (2020).

[4] D. Bini, T. Damour, A. Geralico, S. Laporta, and P. Mastrolia, Gravitational scattering at the seventh order in G: Nonlocal contribution at the sixth post-Newtonian accuracy, Phys. Rev. D **103**, 044038 (2021).

[5] R. A. Porto, The tune of love and the Nature(ness) of spacetime, Fortschr. Phys. **64**, 723 (2016).

[6] G. Kälin and R. A. Porto, From boundary data to bound states, J. High Energy Phys. 01 (2020) 072.

[7] G. Kälin, Z. Liu, and R. A. Porto, Conservative Dynamics of Binary Systems to Third Post-Minkowskian Order from the Effective Field Theory Approach, Phys. Rev. Lett. **125**, 261103 (2020).

[8] Z. Liu, R. A. Porto, and Z. Yang, Spin effects in the effective field theory approach to post-Minkowskian conservative dynamics, arXiv:2102.10059.

[9] Z. Bern, C. Cheung, R. Roiban, C.-H. Shen, M. P. Solon, and M. Zeng, Scattering Amplitudes and the Conservative Hamiltonian for Binary Systems at Third Post-Minkowskian Order, Phys. Rev. Lett. **122**, 201603 (2019).

[10] Z. Bern, C. Cheung, R. Roiban, C.-H. Shen, M. P. Solon, and M. Zeng, Black hole binary dynamics from the double copy and effective theory, J. High Energy Phys. 10 (2019) 206.

[11] Z. Bern, A. Luna, R. Roiban, C.-H. Shen, and M. Zeng, Spinning black hole binary dynamics, scattering amplitudes and effective field theory, arXiv:2005.03071.

[12] Z. Bern, J. P.-Martinez, R. Roiban, E. Sawyer, and C.-H. Shen, Leading nonlinear tidal effects and scattering amplitudes, arXiv:2010.08559.

[13] Z. Bern, J. P.-Martinez, R. Roiban, M. S. Ruf, C.-H. Shen, M. P. Solon, and M. Zeng, Scattering amplitudes and conservative binary dynamics at $\mathcal{O}(G^4)$, Phys. Rev. Lett. **126**, 171601 (2021).

[14] T. Damour, Radiative contribution to classical gravitational scattering at the third order in G, Phys. Rev. D **102**, 124008 (2020).

[15] P. D. Vecchia, C. Heissenberg, R. Russo, and G. Veneziano, The eikonal approach to gravitational scattering and radiation at $\mathcal{O}(G^3)$, arXiv:2104.03256.

[16] M. van de Meent, Gravitational self-force on generic bound geodesics in Kerr spacetime, Phys. Rev. D **97**, 104033 (2018).

[17] L. Barack, A. Ori, and N. Sago, Frequency-domain calculation of the self force: The high-frequency problem and its resolution, Phys. Rev. D **78**, 084021 (2008).

[18] S. Hopper and V. Cardoso, Scattering of point particles by black holes: Gravitational radiation, Phys. Rev. D **97**, 044031 (2018).

[19] S. Hopper, Unbound motion on a Schwarzschild background: Practical approaches to frequency domain computations, Phys. Rev. D **97**, 064007 (2018).

[20] L. Barack and M. Colleoni, T. Damour, S. Isoyama, and N. Sago, Self-force effects on the marginally bound zoom-whirl orbit in Schwarzschild spacetime, Phys. Rev. D **100**, 124015 (2019).

[21] S. R. Dolan and L. Barack, Self-force via m-mode regularization and 2+1D evolution. iii. Gravitational field on Schwarzschild spacetime, Phys. Rev. D **87**, 084066 (2013).

[22] A. Pound, C. Merlin, and L. Barack, Gravitational self-force from radiation-gauge metric perturbations, Phys. Rev. D **89**, 024009 (2014).

[23] L. Barack and P. Giudice, Time-domain metric reconstruction for self-force applications, Phys. Rev. D **95**, 104033 (2017).

[24] I. Racz and G. Z. Toth, Numerical investigation of the late-time Kerr tails, Classical Quant. Grav. **28**, 195003 (2011).

[25] A. Zenginoğlu, G. Khanna, and L. M. Burko, Intermediate behavior of Kerr tails, Gen. Relativ. Gravit. **46**, 1672 (2014).

[26] E. Harms, S. Bernuzzi, and B. Brügmann, Numerical solution of the $2+1$ Teukolsky equation on a hyperboloidal and horizon penetrating foliation of Kerr and application to late-time decays, Classical Quant. Grav. **30**, 115013 (2013).

[27] C. Merlin, A. Ori, L. Barack, A. Pound, and M. van de Meent, Completion of metric reconstruction for a particle orbiting a Kerr black hole, Phys. Rev. D **94**, 104066 (2016).

[28] P. L. Chrzanowski, Vector potential and metric perturbations of a rotating black hole, Phys. Rev. D **11**, 2042 (1975).

[29] R M. Wald, Construction of Solutions of Gravitational, Electromagnetic, or Other Perturbation Equations from Solutions of Decoupled Equations, Phys. Rev. Lett. **41**, 203 (1978).

[30] R. M. Wald, On perturbations of a Kerr black hole, J. Math. Phys. (N.Y.) **14**, 1453 (1973).

[31] S. R. Green, S. Hollands, and P. Zimmerman, Teukolsky formalism for nonlinear kerr perturbations, Classical Quant. Grav. **37**, 075001 (2020).

[32] L. Barack and A. Ori, Gravitational self-force and gauge transformations, Phys. Rev. D **64**, 124003 (2001).

[33] T. S. Keidl, J. L. Friedman, and A. G. Wiseman, On finding fields and self-force in a gauge appropriate to separable wave equations, Phys. Rev. D **75**, 124009 (2007).

[34] T. S. Keidl, A. G. Shah, J. L. Friedman, D.-H. Kim, and L. R. Price, Gravitational self-force in a radiation gauge, Phys. Rev. D **82**, 124012 (2010).

[35] T. S. Keidl, A. G. Shah, J. L. Friedman, D.-H. Kim, and L. R. Price, Gravitational self-force in a radiation gauge, Phys. Rev. D **90**, 109902 (2014).

[36] C. O. Lousto and B. F. Whiting, Reconstruction of black hole metric perturbations from the Weyl curvature, Phys. Rev. D **66**, 024026 (2002).

[37] L. Barack, Late time decay of scalar, electromagnetic, and gravitational perturbations outside rotating black holes, Phys. Rev. D **61**, 024026 (1999).

[38] R. Haas, Scalar self-force on eccentric geodesics in Schwarzschild spacetime: A time-domain computation, Phys. Rev. D **75**, 124011 (2007).

[39] R. Haas, Time domain calculation of the electromagnetic self-force on eccentric geodesics in Schwarzschild spacetime, arXiv:1112.3707.

[40] K. Martel, Gravitational wave forms from a point particle orbiting a Schwarzschild black hole, Phys. Rev. D **69**, 044025 (2004).

[41] L. Barack and N. Sago, Gravitational self-force on a particle in eccentric orbit around a Schwarzschild black hole, Phys. Rev. D **81**, 084021 (2010).

[42] C. O'Toole (private communication).

[43] C. O'Toole, A. Ottewill, and B. Wardell, Characteristic formulation of the Regge-Wheeler and Zerilli Green functions, arXiv:2010.15818.

[44] R. L.-Aleman, G. Khanna, and J. Pulli, Perturbative evolution of particle orbits around Kerr black holes: Time domain calculation, Classical Quant. Grav. **20**, 3259 (2003).

[45] G. Khanna, Teukolsky evolution of particle orbits around Kerr black holes in the time domain: Elliptic and inclined orbits, Phys. Rev. D **69**, 024016 (2004).

[46] L. M. Burko, G. Khanna, and A. Zenginoğlu, Cauchy-horizon singularity inside perturbed Kerr black holes, Phys. Rev. D **93**, 041501(R) (2016).

[47] L. M. Burko and G. Khanna, Linearized stability of extreme black holes, Phys. Rev. D **97**, 061502(R) (2018).

[48] L. M. Burko and G. Khanna, Marolf-ori singularity inside fast spinning black holes, Phys. Rev. D **99**, 081501(R) (2019).

[49] S. Chandrasekhar, On the equations governing the perturbations of the Schwarzschild black hole, Proc. R. Soc. A **343**, 289 (1975).

[50] M. van de Meent (private communication).

[51] L. Barack, Late time dynamics of scalar perturbations outside black holes. 2. Schwarzschild geometry, Phys. Rev. D **59**, 044017 (1999).

[52] Z. Nasipak, T. Osburn, and C. R. Evans, Repeated faint quasinormal bursts in extreme-mass-ratio inspiral waveforms: Evidence from frequency-domain scalar self-force calculations on generic Kerr orbits, Phys. Rev. D **100**, 064008 (2019).

[53] J. Thornburg, B. Wardell, and M. van de Meent, Excitation of Kerr quasinormal modes in extreme–mass-ratio inspirals, Phys. Rev. Research **2**, 013365 (2020).

[54] M. van de Meent, The mass and angular momentum of reconstructed metric perturbations, Classical Quant. Grav. **34**, 124003 (2017).

[55] L. Barack, Gravitational self force in extreme mass-ratio inspirals, Classical Quant. Grav. **26**, 213001 (2009).

[56] S. R. Dolan, Superradiant instabilities of rotating black holes in the time domain, Phys. Rev. D **87**, 124026 (2013).

[57] C. O. Lousto, A time-domain fourth-order-convergent numerical algorithm to integrate black hole perturbations in the extreme-mass-ratio limit, Classical Quantum Gravity **22**, S543 (2005).